communications biology

Article

https://doi.org/10.1038/s42003-024-07125-1

Helicobacter pylori outer membrane vesicles directly promote Aβ aggregation and enhance Aβ toxicity in APP/PS1 mice

Dongli Meng[1,2,8], Yiwen Lai[1,8], Lun Zhang[1,3], Wenting Hu[1,4], Hui Wei[1], Cuiping Guo[1], Xiaopeng Jing[3], Huan Zhou[1], Rui Xiao[1], Liping Zhu[1], Shengquan Luo[1], Zhendong Xu[1], Yu Chen[5], Xiaochuan Wang[1,6], Rong Liu[1,5,6,7] ✉ & Ji Zeng[3] ✉

Helicobacter pylori (*H. pylori*) infection has been found associated with Alzheimer's disease (AD) with unclear mechanisms. Outer Membrane Vesicles (OMVs) are spherical particles secreted by Gram-negative bacteria. Here we explore the effect of *H. pylori* OMVs on Aβ aggregation and toxicity. We show intraperitoneally-injected *H. pylori* OMVs enter the brain and co-localize with Aβ plaques in APP/PS1 mice, accompanied by aggravated Aβ pathology, exacerbated cognitive deficits and synaptic impairment, indicating that *H. pylori* OMVs promote β-amyloidosis and AD development. The in vitro results further identify that *H. pylori* OMVs significantly accelerate Aβ aggregation and increase Aβ-induced neurotoxicity. Through lipidomic analysis, we reveal that lipid components, particularly LPC 18:0 in *H. pylori* OMVs accelerate Aβ aggregation and enhance Aβ neurotoxicity. Moreover, *H. pylori* OMVs-enhanced Aβ neurotoxicity is mediated by Ca^{2+}. These findings reveal a mechanism of *H. pylori* OMVs in accelerating AD development in which the bacterial OMVs-originated lipid components play a key role in promoting Aβ aggregation and neurotoxicity.

Alzheimer's disease (AD), the most prevalent type of dementia among the elderly, has become one of the major social and economic burdens worldwide[1,2]. Senile plaques composed of amyloid β-peptide (Aβ) and neurofibrillary tangles formed by hyperphosphorylated tau are the two pathological hallmarks of AD[3]. Accumulating evidence supports that Aβ deposition plays a pivotal role in the pathogenesis of AD[4], during which a critical step is the assembly of monomeric Aβ into oligomers and subsequent fibrils with a cross β-sheet structure; these aggregates then initiate a cascade of events driving synapse loss, neuronal death and cognitive impairment[5,6]. Although lots of research has been conducted to elucidate the pathogenesis of AD, the specific causes of the disease remain largely unknown. Over the past three decades, there has been constant postulation regarding the infectious etiology of AD[7–9]. The "microbial hypothesis" suggests that chronic infection with viral, bacterial, and/or fungal pathogens may promote AD development[10–12].

Helicobacter pylori (*H. pylori*) is a gram-negative, microaerophilic bacterium that colonizes the gastric mucosa of one-half of the world's population[13]. Several studies indicated an intrinsic link between *H. pylori* infection and AD[14–16]. Beydoun et al. reported a positive association between *H. pylori* seropositivity and AD mortality in a large national retrospective cohort study[17]. In a clinical study, Kountouras et al. found that the histologic prevalence of *H. pylori* infection was significantly higher in AD patients compared with age-matched controls (88% vs 46.7%, respectively), and eradicating *H. pylori* infection may delay AD progression at early disease stages[18,19]. ApoE4, a common genetic risk factor for AD, increased particularly in *H. pylori*-positive AD than in *H. pylori*-negative AD patients[20]. Furthermore, when the human gastric cells were incubated with the *H. pylori* peptide Hp_{2-20}, several genes directly related to AD such as *APP*, *APOE*, *PSEN1*, and *PSEN2* were found to be up-regulated[21]. Our group previously reported that peritoneal injection of *H. pylori* filtrate from cultured bacteria increased brain level of Aβ, induced tau

[1]Department of Pathophysiology, School of Basic Medicine, Key Laboratory of Education Ministry of China/Hubei Province for Neurological Disorders, Tongji Medical College, Huazhong University of Science and Technology, Wuhan, China. [2]Sino-UK Joint Laboratory of Brain Function and Injury of Henan Province, Department of Physiology and Pathophysiology, Xinxiang Medical University, Xinxiang, China. [3]Department of Clinical Laboratory, Wuhan Fourth Hospital, Wuhan, China. [4]Department of Pathology, Peking University Shenzhen Hospital, Shenzhen, China. [5]Department of Pediatrics, Tongji Hospital, Tongji Medical College, Huazhong University of Science and Technology, Wuhan, China. [6]Shenzhen Huazhong University of Science and Technology Research Institute, Shenzhen, China. [7]Institute for Brain Research, Wuhan Center of Brain Science, Huazhong University of Science and Technology, Wuhan, China. [8]These authors contributed equally: Dongli Meng, Yiwen Lai. ✉e-mail: rong.liu@hust.edu.cn; whzjmicro@163.com

hyperphosphorylation, and impaired cognition in rats[22,23]. However, the molecular mechanism by which *H. pylori* filtrate induced AD-like pathology is still unknown.

Outer membrane vesicles (OMVs) are spherical, bilayered membranous structures with average diameters of 20–250 nm, which are secreted by a wide variety of gram-negative bacteria during all stages of bacterial growth[24,25]. With bacterial-originated lipids, proteins, lipopolysaccharides (LPS), DNAs, RNAs, metabolites, and lots of signaling molecules equipped, OMVs exert several biological functions such as cell-to-cell signal transduction, toxins transferring, and immune response elicitation in host cells[26–28]. The presence of *H. pylori* OMVs has been reported in the blood of chronic *H. pylori*-infected mice[29]. Numerous in vivo studies have shown that OMVs administered peripherally can be detected in the brain in mice[30–34]. Recently, two independent studies reported that peripheral administration of *H. pylori* OMVs resulted in its detection in the brain, which coincided with astrocyte reactivity and neuronal damage[35,36]. Herein, we focused on the direct effect of *H. pylori* OMVs on β-amyloidosis in an AD mouse model and in vitro. We injected *H. pylori* OMVs intraperitoneally into APP/PS1 mice and found *H. pylori* OMVs co-localized with Aβ plaques, suggesting a direct link between *H. pylori* OMVs and Aβ pathology. *H. pylori* OMVs treatment for 6 months exacerbated Aβ deposition, aggravated cognitive deficits, and synaptic impairment in APP/PS1 mice. Further in vitro study demonstrated that *H. pylori* OMVs significantly enhanced Aβ aggregation and Aβ-induced neurotoxicity. In addition, lipidomic analysis revealed lipid component LPC was abundant in *H. pylori* OMVs. In particular, LPC 18:0 in *H. pylori* OMVs significantly accelerated Aβ aggregation and enhanced Aβ neurotoxicity. Moreover, we found that *H. pylori* OMVs-enhanced Aβ toxicity was mediated by Ca^{2+}. This study discloses a mechanism of *H. pylori* infection in promoting AD pathologies, and reveals a direct pathway through OMVs-delivery for peripheral colonized bacteria to transfer pathogenic substance into the brain and induce disorders in the central nervous system.

Results

Intraperitoneally administered *H. pylori* OMVs co-localize with Aβ plaques and exacerbate Aβ deposition in brain of APP/PS1 mice

H. pylori OMVs and *E. coli* OMVs were isolated from culture supernatants of *H. pylori* strain ATCC49503 and *E. coli* strain ATCC 25922 using μLtracentrifugation. We first characterized the isolated OMVs. Transmission electron microscopy (TEM) and nanoparticle tracking analysis (NTA) demonstrated that both *H. pylori* OMVs and *E. coli* OMVs remained an intact structure with a 100–200 nm diameter (Fig. 1A, B). Western blotting analysis showed that urease B (UreB), the major virulence protein of *H. pylori* is present in *H. pylori* OMV, rather than in *E. coli* OMVs (Fig. 1C).

To determine whether OMVs could migrate to the brain, 10 μg of fluorescent dye DiD-labeled *H. pylori* OMVs or *E. coli* OMVs were administered intraperitoneally to APP/PS1 mice. Mice were sacrificed, and the brains were sliced for imaging after 48 h. Laser confocal microscopy images showed both *H. pylori* OMVs or *E. coli* OMVs labeled by DiD (red) in the brain slices, indicating OMV entered the brain. Besides, using the dendritic marker MAP-2 to identify neurons and Aβ antibody 4G8 to probe amyloid plaques, we found that OMVs (red) were co-localized with amyloid plaques (green) in the hippocampus of APP/PS1 mice (Fig. 1D).

We further assessed the effect of OMVs on Aβ deposition. Female APP/PS1 mice (3-month old) were intraperitoneally injected with *H. pylori* OMVs, *E. coli* OMVs or PBS as control every other day for 6 months, and wild-type female mice (3-month old) were injected with PBS as the normal control. In female APP/PS1 mice, amyloid plaques begin to deposit in the brain at about 3 months and increase in size and number with age, therefore we choose female APP/PS1 and age-matched wild type mice at 3-month before Aβ plaque formation to determine the effect of bacterial OMVs on amyloidosis. 6 months later, mice were sacrificed at the end of behavioral tests. Amyloid plaque was quantified by staining with thioflavin-S. The results showed that thioflavin-S-positive plaques significantly increased in the hippocampus of *H. pylori* OMVs-injected APP/PS1 mice compared with PBS- or *E. coli* OMVs-injected mice (Fig. 1E, F), indicating *H. pylori* OMVs significantly increased the amyloid plaque burden. For evaluating the Aβ levels, we prepared the PBS-soluble and insoluble (soluble in formic acid, FA) fractions from mouse hippocampal tissue to detect $Aβ_{40}$ and $Aβ_{42}$ levels by ELISA. The results showed a significant increase in $Aβ_{42}$ level in the insoluble fraction of the hippocampus of *H. pylori* OMVs-injected mice (Fig. 1G). We next examined the levels of proteins involved in amyloidogenic processing of APP in the hippocampus by Western blotting. The level of APP phosphorylation at T668 was also detected because of its significant promotional effect on APP cleavage[37]. The results showed there was no difference in the levels of APP, APP phosphorylation at T668, β-cleavage product sAPPβ, β-site APP cleaving enzyme 1 (BACE1) and presenilin 1(PS1) in hippocampus (Fig. 1H, I) among the three groups, excluding the possibility that the severer amyloid plaque burden in *H. pylori* OMVs-injected mice was caused by increased production of Aβ. Thus, peripherally administrated OMVs may enter the brain, co-localize with Aβ plaques, and exacerbate Aβ deposition without influencing Aβ production in APP/PS1 mice.

H. pylori OMVs exacerbate cognitive deficits and promote synaptic impairment in APP/PS1 mice

To evaluate the effect of *H. pylori* OMVs on the cognitive function of the mouse model, Morris Water Maze (MWM) was performed to test spatial learning and memory. APP/PS1 mice injected with *H. pylori* OMVs showed similar performances compared with control and *E. coli* OMVs-injected group in the learning phase (Fig. 2B). However, when the platform was placed in the opposite quadrant (Reversal MWM), in learning phase trial, as shown in Fig. 2C, D, the escape latency of *H. pylori* OMVs -injected APP/PS1 mice was significantly increased on the last day of learning compared with those of the PBS- or *E. coli* OMVs-injected mice. In the probe trial after the platform was removed, time spent in the target quadrant and numbers of crossing platform of *H. pylori* OMVs-injected APP/PS1 mice significantly decreased compared with those of the PBS- or *E. coli* OMVs-injected mice (Fig. 2E, F), indicating severer impairment in learning and memory. The swimming speeds did not differ among control and OMVs-treated groups (Fig. 2G). Next, contextual discrimination test was performed to assess the ability of mice to discriminate two similar conditioning contexts, A and B (Fig. 2H), to further confirm the cognitive deficits in *H. pylori* OMVs-injected APP/PS1 mice. On the first three days, mice were exposed only to context A and received a foot-shock after 180 s each day. The results showed APP/PS1 mice injected with *H. pylori* OMVs acquired fear memory to A similar to control mice or *E. coli* OMVs-injected mice (Fig. 2I). On days 4 and 5, the ability of mice to distinguish context A and B was examined by exposing mice to context A and B in a randomized order, and neither group received a foot-shock in A or B. All groups of APP/PS1 mice exhibited no distinguishing to context A and B (Fig. 2J). Animals were then daily exposed to both contexts with a single foot-shock received only in context A for seven days. Over the seven testing days, APP/PS1 mice injected with PBS or *E. coli* OMVs progressively increased their discrimination ratio, whereas APP/PS1 mice injected with *H. pylori* OMVs showed no improvement (Fig. 2K). On the last day, PBS and *E. coli* OMVs-treated mice could discriminate the two chambers, whereas *H. pylori* OMVs-treated APP/PS1 mice failed (Fig. 2L). Besides, all APP/PS1 mice showed severe cognitive deficits compared with age-matched WT mice in both behavior tests. Taken together, our study suggested that *H. pylori* OMVs exacerbated cognitive deficits in APP/PS1 mice. The severe cognitive impairment in *H. pylori* OMVs-treated mice was consistent with severe Aβ aggregation and deposition in the brains of these mice.

Aggregated Aβ exerts toxicity to synapses and neurons through multiple pathways[38], to disclose the underlying mechanism for the severer cognitive deficits in *H. pylori* OMVs-treated mice, synaptic proteins levels were compared among the different groups. Western blotting results showed levels of PSD95 and GluA1 were significantly decreased in the hippocampus of *H. pylori* OMVs -injected APP/PS1 mice (Fig. 2M, N). Immunofluorescence staining results showed that PSD95

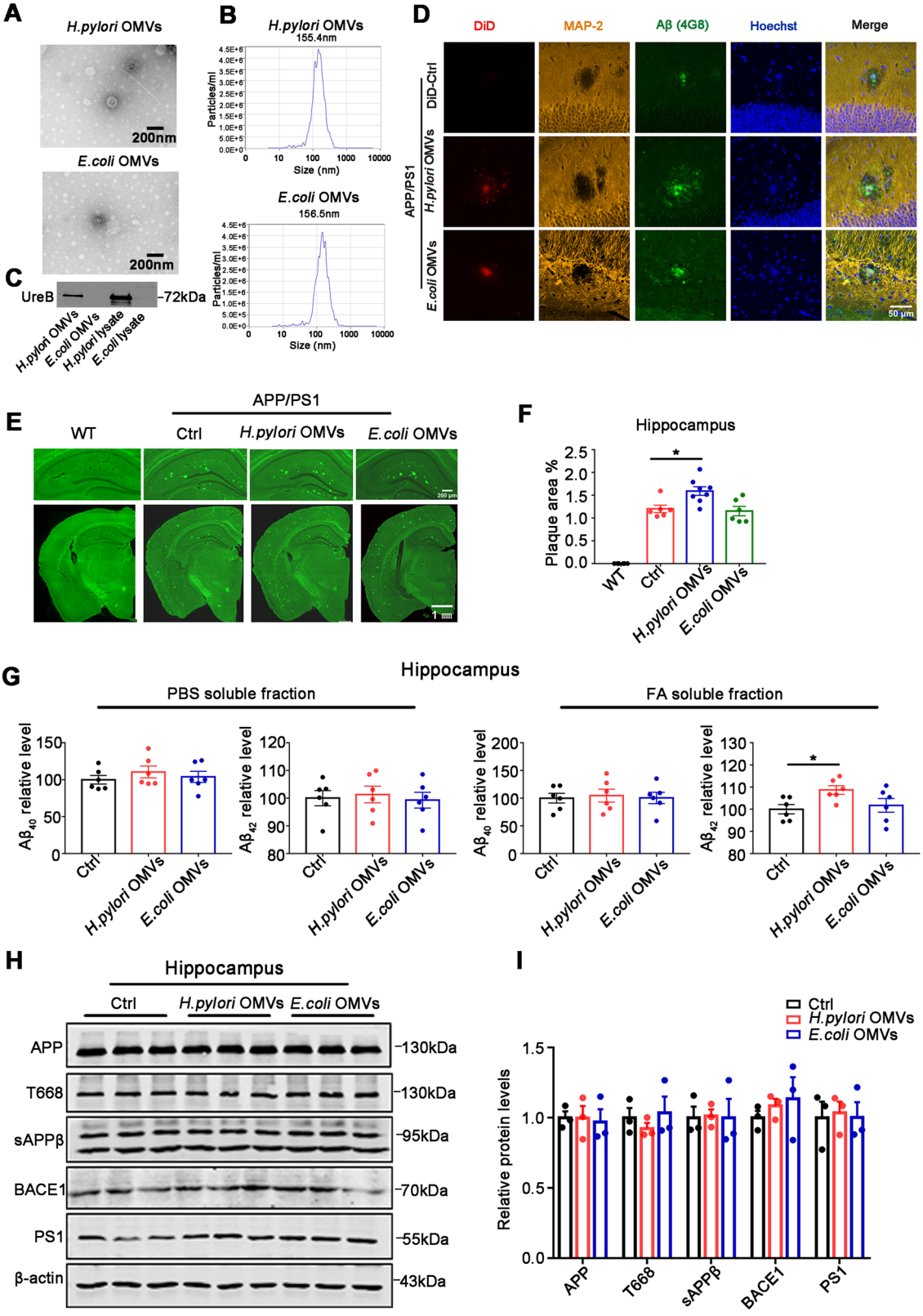

immunofluorescence signaling was decreased in the hippocampus of APP/PS1 mice intraperitoneally injected with *H. pylori* OMVs compared with other two groups (Fig. S1A, B), indicating *H. pylori* OMVs promote synaptic impairment in APP/PS1 mice. The number of dendritic spines was also decreased in the hippocampus of *H. pylori* OMVs-injected APP/PS1 mice (Fig. 2O, P). However, *H. pylori* OMVs did not increase neuronal death in APP/PS1 mice (Fig. S2A–E). Besides, peripherally administrated *H. pylori* OMVs increased tau hyperphosphorylation levels (Fig. S3A, B) and enhanced neuroinflammation in APP/PS1 mice (Fig. S4A–D). Together, these results suggested that *H. pylori* OMVs aggravated cognitive deficits and synaptic impairment in AD mice models.

Fig. 1 | Peripherally administrated *H. pylori* OMVs migrate to the brain, co-localize with Aβ plaques and exacerbate Aβ deposition in brain of APP/PS1 mice. **A** Representative TEM images of *H. pylori* OMVs and *E. coli* OMVs. **B** Size distribution profiles of *H. pylori* OMVs or *E. coli* OMVs detected by nanoparticle tracking analysis (NTA). **C** Western blotting analysis of UreB in OMVs. **D** APP/PS1 mice were intraperitoneally injected with DiD-labeled *H. pylori* OMVs or *E. coli* OMVs. Representative immunostaining images reveal that both *H. pylori* OMVs (Red) and *E. coli* OMVs (Red) co-localize with Aβ plaques (4G8, Green) in the hippocampus of APP/PS1 mice following 48 h of injection. Nuclei were stained with Hoechst (Blue). **E** Representative images of Aβ plaque staining with THS (Green) in brains of WT, APP/PS1, APP/PS1 injected with *H. pylori* OMVs, and APP/PS1 injected with *E. coli* OMVs mice after 6 months. Scale bars are as indicated in each panel. **F** Quantification of THS-positive plaques in the hippocampus of APP/PS1 mice (3 mice per group and 2–3 slices per mouse). **G** $A\beta_{40}$ and $A\beta_{42}$ levels in PBS soluble or formic acid (FA) soluble fractions in the hippocampus of APP/PS1 mice detected by ELISA ($n = 6$). Data are shown as mean ± SEM, one-way ANOVA with Tukey's test, $^*p < 0.05$. **H**, **I** Immunoblots and quantification for total APP, phosphorylated APP at T668, sAPPβ, BACE1, and PS1 in the hippocampus of APP/PS1 mice. No difference was observed among APP/PS1, APP/PS1 with *H. pylori* OMVs, and APP/PS1 with *E. coli* OMVs groups. Samples of Fig. 1E–I were from the same experiment.

H. pylori OMVs accelerate Aβ aggregation and enhance Aβ-induced neurotoxicity in vitro

Based on the observation that *H. pylori* OMVs aggravated Aβ deposition in animal experiments, we next examined whether *H. pylori* OMVs had direct effect of promoting Aβ aggregation in vitro. ThT can specifically bind to cross β-sheet structures in amyloid fibrils and emit fluorescence[39]. $A\beta_{42}$ monomers were incubated alone or with *H. pylori* OMVs/*E. coli* OMVs at 37 °C for 8 h. ThT assay showed *H. pylori* OMVs increased ThT fluorescence intensity compared with Aβ alone or Aβ + *E. coli* OMVs, and in a dose-dependent manner (Fig. 3A, B), indicating that *H. pylori* OMVs accelerated amyloid formation of $A\beta_{42}$. We further used TEM to visualize the morphologic changes of the end-point incubation products. $A\beta_{42}$ monomers incubation alone or with *E. coli* OMVs mostly assembled into aggregates and little fibrils at the end of incubation. However, obvious amyloid fibrils were observed in the presence of *H. pylori* OMVs (Fig. 3C). When the incubation time extended to 1 week, amyloid fibrils were observed in all three groups, however, fibrils formed by $A\beta_{42}$ incubated with *H. pylori* OMVs were more obvious and bolder compared with those formed by $A\beta_{42}$ incubated alone or with *E. coli* OMVs (Fig. 3C). *H. pylori* OMVs were tightly attached with the fibrils, indicating *H. pylori* OMVs may act as a catalytic surface for accelerating Aβ aggregation and fibrils formation. In addition, the fibers appeared to cause morphological changes of *H. pylori* OMVs, from typically spherical vesicles to irregularly shaped vesicles (Fig. 3C) that have blebs protruding around the vesicles, which was similar to the changes of large unilamellar vesicles (LUV, a simple biomimetic model alternative to in vivo natural cell membranes) incubated with fibrillizing $A\beta_{42}$[40]. Taken together, *H. pylori* OMVs accelerated Aβ aggregation in vitro. To further confirm the interaction of Aβ with *H. pylori* OMVs, $A\beta_{42}$ monomers and *H. pylori* OMVs were labeled with FITC (Aβ-FITC, green) and fluorescent dye DiD (OMVs-DiD, red), respectively. Laser confocal microscopy images identified the co-localization of Aβ-FITC and OMVs-DiD (Fig. 3D), indicating Aβ can interact with *H. pylori* OMVs. Nanoparticles have been shown to bind amyloidogenic peptides on their surface, inducing conformational changes that facilitate amyloid aggregation and fibril growth via a surface-assisted heterogenous nucleation mechanism[41–43]. Therefore, it is reasonable to speculate that *H. pylori* OMVs can capture Aβ on their surface to promote the formation of Aβ fibril.

Since *H. pylori* OMVs accelerated Aβ aggregation, we next examined the effects of *H. pylori* OMVs on Aβ-induced neurotoxicity. The same amount of $A\beta_{42}$ monomers at the same concentration (1 μM) were pre-incubated alone or with *H. pylori* OMVs/*E. coli* OMVs at 37 °C for 8 h to form different Aβ aggregates. Primary neurons were treated with the above Aβ aggregates for 24 h. In our experiment, we set the concentration of Aβ monomer to 1 μM at which concentration Aβ monomers and later formed aggregates during the whole treatment showed no significant cytotoxicity (data not shown). Using the neuronal marker MAP-2 showing the neuronal morphology (green), we found that *H. pylori* OMVs-incubated Aβ aggregates dramatically damaged neuronal dendrites compared with Aβ aggregates/OMVs alone or *E. coli* OMVs-incubated Aβ aggregates (Fig. 3E, F). LDH cytotoxicity assay showed *H. pylori* OMVs-incubated Aβ aggregates significantly increased the neurotoxicity compared with other treatments (Fig. 3G). We also examined the intracellular ROS production (detected by DCFH-DA). The results showed that *H. pylori* OMVs-incubated Aβ aggregates significantly increased intracellular ROS production compared with Aβ aggregates alone or *E. coli* OMVs-incubated Aβ aggregates, which further elucidated the findings of cytotoxicity assay (Fig. S5A, B). Besides, using the neuronal marker MAP-2 showing the neuronal morphology (cyan), we found that *H. pylori* OMVs and $A\beta_{42}$ alone adhered to the cell membrane of neurons without inducing neuron damage. However, when applying incubation mixture of *H. pylori* OMV with $A\beta_{42}$, neurons were damaged severely (Fig. 3H). Furthermore, Western blotting showed the level of post-synaptic PSD95 was dramatically decreased in neurons treated with *H. pylori* OMVs-incubated Aβ aggregates (Fig. 3I–K). Collectively, these data indicated that *H. pylori* OMVs significantly enhanced Aβ-induced neurotoxicity.

Lipid components in *H. pylori* OMV contribute to the enhancement of Aβ neurotoxicity

H. pylori OMVs contain proteins, RNAs, DNAs and lipids, we next identified which components in *H. pylori* OMVs were responsible for enhancing Aβ neurotoxicity. *H. pylori* OMVs were underwent five freezing-thawing cycles and given the following treatments before incubated with Aβ monomers: proteinase (to degrade proteins), RNase (to degrade RNAs), DNase (to degrade DNAs) and silica (to deplete lipids)[44,45]. Then the incubation mixture of above treated *H. pylori* OMVs with Aβ was applied to primary neurons for 24 h. Western blotting showed that *H. pylori* OMVs after repeated freezing-thawing still enhanced Aβ synaptotoxicity, indicating that the effect was not dependent on the intact structure of *H. pylori* OMVs. In the different components excluding experiments, only pre-treatment with silica prevented *H. pylori* OMVs-enhanced synaptotoxicity of Aβ (Fig. 4A–C), suggesting that *H. pylori* OMVs-enhanced Aβ toxicity was most likely attributed to lipid components in *H. pylori* OMVs.

To further clarify the lipid candidate which participates in this process, next, we performed lipidomics to analyze lipid profiles of *H. pylori* OMVs and *E. coli* OMVs using μLtra-high performance liquid chromatography-Tandem mass spectrometry (UPLC-MS/MS). A total of 43 lipid subclasses and 459 lipids were detected, of which TG (triglyceride), Cer-NS (ceramide), SM (sphingomyelin), LPC (lysophosphatidylcholine) were in the majority (Fig. 4D, E). A total of 147 differential lipids were identified between *H. pylori* OMVs and *E. coli* OMVs based on $p < 0.05$, and FC > 2 or FC < 0.5. Of these, 76 lipids were upregulated and 71 lipids were downregulated in *H. pylori* OMVs (Fig. 4F). We further analyzed the lipids in the top-20 difference multiplex, and found that lipid subclass lysophosphatidylcholine (LPC), especially LPC 15:0 and LPC 18:0 were significantly upregulated in *H. pylori* OMVs (Fig. 4G). KEGG enrichment analysis showed that these differential lipids were mainly associated with glycerophospholipid metabolism, autophagy pathway and glycine, serine and threonine metabolic pathway (Fig. 4H). Together, these data suggested that lipid components in *H. pylori* OMVs were involved in enhancing Aβ neurotoxicity.

LPC 18:0 in *H. pylori* OMVs accelerates Aβ aggregation and enhances Aβ neurotoxicity in vitro and in brain of APP/PS1 mice

Lipidomics results showed that LPC 15:0 and LPC 18:0 were largely abundant in *H. pylori* OMVs, thus we next investigated whether they were responsible for enhancing Aβ aggregation and neurotoxicity of *H. pylori* OMVs. We first examined their effect on Aβ aggregation and toxicity

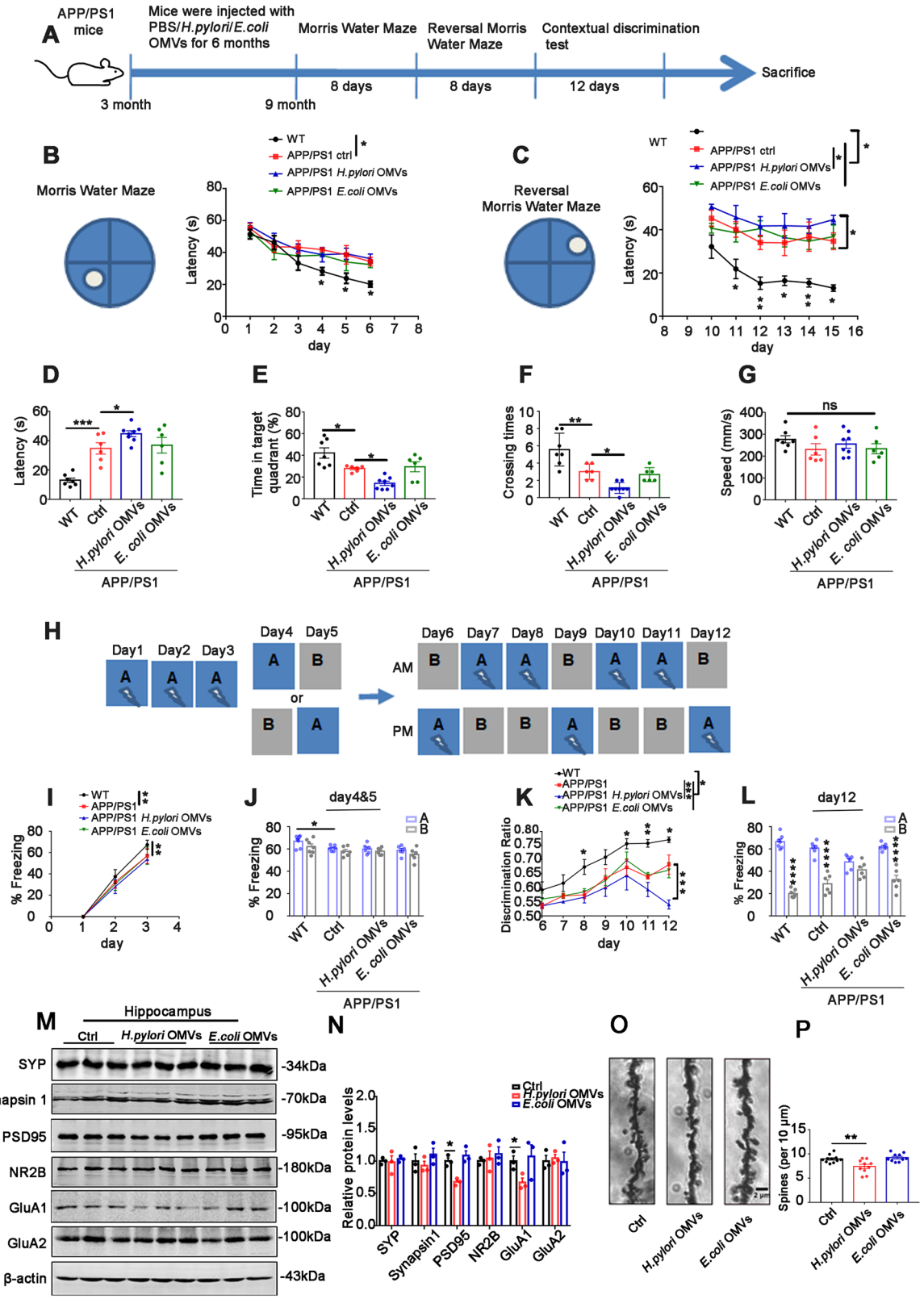

in vitro. ThT assay showed both LPC 15:0 and LPC 18:0 promoted Aβ aggregation, however, the effect of LPC 18:0 was more significant in a dose-dependent manner (Figs. 5A and S6). We thus examined the effect of LPC 18:0 on Aβ-induced neurotoxicity in primary neurons. Western blotting showed level of PSD95 was significantly decreased in neurons treated with LPC 18:0-incubated Aβ aggregates compared with Aβ aggregates alone (Fig. 5B, C). These data indicated that LPC 18:0 in *H. pylori* OMVs was the possible key component responsible for accelerating Aβ aggregation and enhancing Aβ-induced neurotoxicity.

To further confirm this speculation, we injected *H. pylori* OMVs and LPC 18:0 respectively into right hippocampus of 6-month-old female APP/PS1 mice, the other hemisphere was injected with normal saline as control

Fig. 2 | *H. pylori* OMVs exacerbate cognitive deficits and promote synaptic impairment in APP/PS1 mice. **A** Experimental scheme. **B**–**G** The spatial learning ability and memory of WT and APP/PS1 mice were tested in Morris Water Maze (MWM). (WT, $n = 7$, APP/PS1, $n = 6$, *H. pylori* OMVs, $n = 8$, *E. coli* OMVs, $n = 6$). **B** Escape latency to find the hidden platform during training phase in MWM. Mean ± SEM, two-way ANOVA, and Tukey's test, $^{*}p < 0.05$ (WT vs. APP/PS1 at day 4,5,6). **C** Escape latency to find the hidden platform during training phase in reversal MWM. Mean ± SEM, two-way ANOVA, and Tukey's test, $^{*}p < 0.05$ (APP/PS1 vs. APP/PS1 *H. pylori* OMVs at day 15). **D** Escape latency at day 15 in reversal MWM. Mean ± SEM, one-way ANOVA, and Tukey's test, $^{*}p < 0.05$. **E** Percentage of time spent in target quadrant in probe test in reversal MWM. Mean ± SEM, one-way ANOVA, and Tukey's test, $^{*}p < 0.05$. **F** Number of crossing the location of the target platform in probe test in reversal MWM. Mean ± SEM, one-way ANOVA, and Tukey's test, $^{*}p < 0.05$, $^{**}p < 0.01$. **G** Speed of swimming in probe test. **H**–**L** Contextual discrimination test of the mice (WT, $n = 7$, APP/PS1, $n = 6$, *H. pylori* OMVs, $n = 6$, *E. coli* OMVs, $n = 6$). **H** Experimental design of the contextual discrimination test. **I** Percentage of freezing time during the acquisition. Mean ± SEM, two-way ANOVA and Tukey's test, $^{**}p < 0.01$ (WT vs. APP/PS1). **J** Freezing levels in **A**, **B** during the generalization test. Mean ± SEM, one-way ANOVA and Tukey's test, $^{*}p < 0.05$ (WT vs. APP/PS1). **K** Discrimination ratio of mice across the seven days of acquisition. Mean ± SEM, two-way ANOVA and Tukey's test, $^{***}p < 0.001$ (APP/PS1 vs. APP/PS1 *H. pylori* OMVs). **L** Freezing levels in **A**, **B** of mice on the last testing day. Mean ± SEM, one-way ANOVA and Tukey's test, $^{****}p < 0.0001$. **M**, **N** Immunoblots and quantification for synaptic proteins including synaptophysin (SYP), Synapsin I, PSD95, NR2B, GluA1, and GluA2 in the hippocampus of APP/PS1, APP/PS1 with *H. pylori* OMVs, and APP/PS1 with *E. coli* OMVs mice. $n = 3$ per group. Data shown as mean ± SEM, two-way ANOVA and Tukey's test, $^{*}p < 0.05$. **O** Dendritic spines in Golgi-stained slices of hippocampus from APP/PS1 mice injected with PBS, *H. pylori* OMVs or *E. coli* OMVs. Scale bar: 2 μm. **P** Quantification of the spine number (3 mice per group and 3–4 neurons per mouse). Data shown as mean ± SEM, one-way ANOVA and Tukey's test, $^{**}p < 0.01$.

(Fig. 5D). After one week, mice were sacrificed and the brains were sectioned to examine AD pathologies. Amyloid plaque was quantified by staining with thioflavin-S, and synaptic impairment was evaluated by synaptic protein PSD95 immunostaining. We found that thioflavin-S positive plaques were significantly increased in the hemisphere of APP/PS1 mice exposed to *H. pylori* OMVs and LPC 18:0 injection (Fig. 5E, G, H), indicating *H. pylori* OMVs and LPC 18:0 directly increased the amyloid plaque burden. Immunofluorescence staining results showed that PSD95 immunofluorescence signaling was decreased in the hemisphere with *H. pylori* OMVs and LPC 18:0 injection in APP/PS1 mice compared with that in control side (Fig. 5F, I, J), indicating *H. pylori* OMVs and LPC 18:0 promote synaptic impairment. Taken together, these results suggest that LPC 18:0 in *H. pylori* OMVs accelerates Aβ aggregation and enhances Aβ neurotoxicity in vitro and in brain of APP/PS1 mice.

H. pylori OMVs and LPC 18:0-enhanced Aβ toxicity is mediated by Ca^{2+}

The molecular mechanisms leading to synaptotoxicity of Aβ have not been fully elucidated. In neuronal cultures and in vivo, increased intracellular Ca^{2+} levels in response to Aβ play a central role in synapse dysfunction and loss[46]. To examine whether the observed *H. pylori* OMVs-enhanced Aβ toxicity in our study is also mediated by Ca^{2+}, intracellular Ca^{2+} level was measured by Ca^{2+} imaging in neurons treated with OMVs-incubated Aβ aggregates or Aβ aggregates/OMVs alone. The result showed that though Aβ aggregates alone induced elevation of intracellular Ca^{2+} level considerably, *H. pylori* OMVs and Aβ incubation mixture resulted in a more rapid and higher increase of intracellular Ca^{2+} (Fig. 6A and B). To examine extent of the increase in Ca^{2+} induced by OMVs-incubated Aβ aggregates, cultured primary neurons were treated with Aβ aggregates alone and *H. pylori* OMVs-incubated Aβ aggregates, and then 5 μM ionomycin was added to obtain the highest elevation of intracellular Ca^{2+} [47]. Calcium imaging results showed that *H. pylori* OMVs-incubated Aβ aggregates-induced Ca^{2+} elevation reached 80.45% of the maximum, whereas Aβ aggregates-alone induced Ca^{2+} elevation reached only 54.66% of the maximum in primary neurons (Fig. S7). These data indicate the potent effect of *H. pylori* OMVs in promoting Aβ-induced calcium-dependent toxicity. To further confirm this hypothesis, we removed the extracellular Ca^{2+} in culture media and detected the neurotoxicity of *H. pylori* OMVs-incubated Aβ aggregates. Using the neuronal marker MAP-2 showing the neuronal morphology, we observed that *H. pylori* OMVs and Aβ-induced neuronal morphologic damage was rescued by extracellular Ca^{2+} depletion (Fig. 6C). In addition, the significant decrease of synaptic protein PSD95 in neurons treated with *H. pylori* OMVs-incubated Aβ aggregates was also reversed when extracellular Ca^{2+} was removed (Fig. 6D–F). These data collectively indicate that Ca^{2+} is required for *H. pylori* OMVs-enhanced Aβ toxicity. Based on the finding that LPC 18:0 contained in *H. pylori* OMVs contributes to Aβ aggregation and toxicity, we also investigated whether Ca^{2+} was involved in LPC 18:0-enhanced neurotoxicity. Ca^{2+} imaging results showed that incubation mixture of LPC 18:0 and Aβ significantly increased intracellular Ca^{2+} level in neurons compared with Aβ or LPC 18:0 alone, though Aβ and LPC 18:0 alone induced elevation of intracellular Ca^{2+} level (Fig. 6G, H). Besides, decrease of synaptic protein PSD95 in neurons treated with LPC 18:0-incubated Aβ aggregates was also reversed when extracellular Ca^{2+} was removed (Fig. 6I, J). Taken together, *H. pylori* OMVs and LPC 18:0-enhanced Aβ toxicity is mediated by Ca^{2+}.

Discussion

Large amounts of studies have demonstrated an association between AD and microbial infection[7–12]. Microorganisms may play a role in AD development by exerting effects on neuronal cells directly through migrating to the brain, or acting on neuronal cells indirectly through release of toxins, OMVs or pro-inflammatory molecules into blood[48]. *H. pylori* is a causative agent of stomach μLcer and gastric cancer that colonizes in the stomach of approximately 50% of the world's population. Increasing evidences suggest that *H. pylori* is one of the most relevant pathogens associated with AD development[14–16], however the underlying mechanisms remains unknown.

Bacteria shed OMVs containing periplasmic fluid during growth. Several studies have shown the involvement of OMVs in the delivery of bacterial virulence factors of *E. coli*[49], *P. aeruginosa*[50], and *P. gingivalis*[51]. Besides, Wei et al. found that OMVs derived from the feces of AD patients can enter the brain and induce neuroinflammation and tau hyperphosphorylation in mice[30], with the precise etiologic pathogen in the mixed OMVs and detailed mechanisms to be further clarified. Recently, studies have reported that *H. pylori* OMVs administered systemically or orally entered the brain and induced neuroinflammation via activating glial cells[29,35,36]. In the present study, we demonstrated the effects of *H. pylori* OMVs on AD-related pathologies through intraperitoneal injection of OMVs to APP/PS1 mice, and disclosed a novel role of *H. pylori* OMVs in accelerating AD pathologies by directly promoting Aβ aggregation and its neurotoxicity.

First, we explored whether OMVs administered intraperitoneally migrate to the brain in APP/PS1 mice. Both DiD-labeled *H. pylori* OMVs and *E. coli* OMVs were detected in the mouse brain 48 hours after intraperitoneal injection, indicating OMVs entered the brain. This result is consistent with previously published studies showing that orally gavaged Cre recombinase-loaded *H. pylori* OMVs in astrocytes and neurons[35], and intravenously injected fluorescence DiR or cyanine7 (Cy7)-labeled HP-OMVs in the brain of mice[29,36]. In the well-designed experiments of Xie et al., *H. pylori* OMVs were found to enter the brain without destroying BBB. Our data, together with published studies, support the transfer of H. pylori OMVs into the brain.

In our study, the injection of *H. pylori* OMVs persisted for 6 months (from 3-month-old to 9-month-old), this is a long period for mice with a lifespan of about two years. We did this for the following two reasons: 1) For APP/PS1 mice, the amyloidosis was observed at about 3-month-old, and cognitive deficits in the MWM emerged between 6 and 10 months and

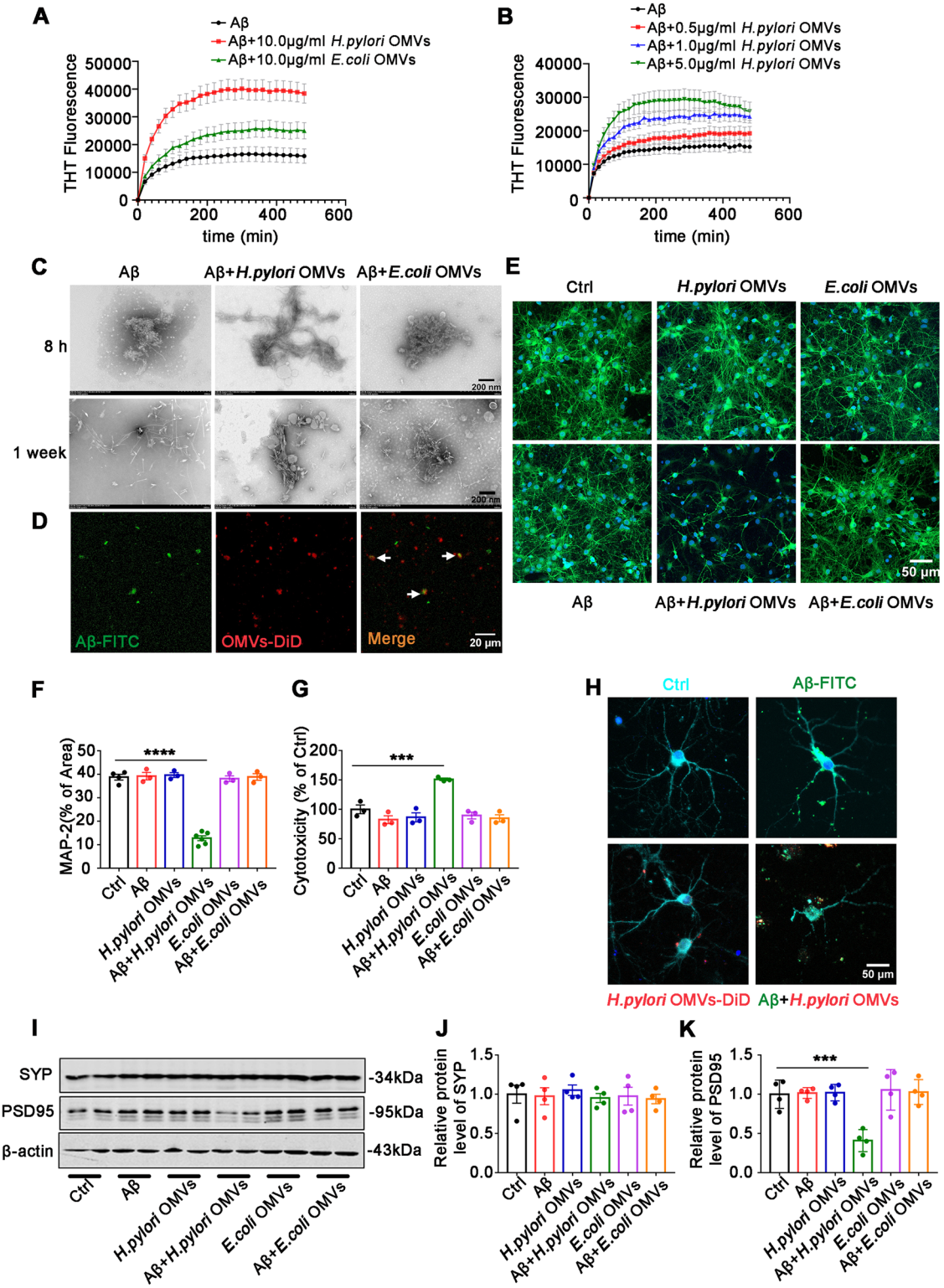

worsen with age[52]; 2) Mice at 3–6 months of age are defined as mature adult, corresponding to human age at 20–30 years old. *H. pylori* is highly prevalent worldwide and usually chronically colonizes the stomach of the patient for long time before diagnosed. To mimic this chronic infection process, we injected OMVs into mice for 6 months. Using Aβ antibody 4G8 to probe amyloid plaques, we found that *H. pylori* OMVs co-localized with amyloid plaques and increased amyloid plaque formation in the brain of APP/PS1 mice. This result is consistent with the previous finding of significantly increased deposition of amyloid plaques in hippocampal CA1 and CA3 regions of App^{NL-G-F} mice gavaged with *H. pylori* OMVs for three weeks. The authors also reported that in wild-type mice, same treatment of *H. pylori* OMVs for three weeks resulted in neuronal loss in hippocampal CA3 region through NeuN staining[35]. In our study, *H. pylori* OMVs only enhanced synaptic damage instead of neuronal loss in APP/PS1 mice. This discrepancy may be due to the difference in mouse models used and the delivery strategy of *H. pylori* OMVs. In line with the increased loss in

Fig. 3 | *H. pylori* OMVs accelerate Aβ aggregation and enhance Aβ-induced neurotoxicity in vitro. A Aggregation kinetics of $A\beta_{42}$ incubated alone or with 10.0 μg/ml *H. pylori* OMVs/*E. coli* OMVs monitored by ThT assay. **B** Aggregation kinetics of $A\beta_{42}$ incubated alone or with different concentration of *H. pylori* OMVs. The averaged data from three replicates and standard deviations are plotted. **C** TEM images showing the end-point products of $A\beta_{42}$ incubated alone or with *H. pylori* OMVs and *E. coli* OMVs k at 37 °C for 8 h and 1 week. Scale bar, 200 nm. **D** Laser confocal microscopy images of incubation mixtures of $A\beta_{42}$ and *H. pylori* OMVs. (green, Aβ-FITC; red, *H. pylori* OMVs-DiD). Scale bar, 20 μm. **E** Cultured primary neurons were treated with PBS, $A\beta_{42}$ aggregates alone, *H. pylori* OMVs-incubated $A\beta_{42}$ aggregates, *H. pylori* OMVs alone, *E. coli* OMVs-incubated $A\beta_{42}$ aggregates, and *E. coli* OMVs alone at 37 °C for 24 h. Neurons were immunostained with antibody against dendritic marker MAP-2 (Green) to show the neuronal morphology. Nuclei were stained with Hoechst (Blue). Scale bar, 50 μm. **F** Quantification of MAP-2 fluorescence signaling in different groups of mice. Data shown as mean ± SEM, one-way ANOVA with Tukey test, $^{****}p < 0.0001$. **G** Cytotoxicity was determined using LDH cytotoxicity assay kit ($n = 3$ for cell samples). Data shown as mean ± SEM, one-way ANOVA with Tukey test, $^{***}p < 0.001$. **H** Fluorescence images showing morphology of neurons treated with PBS, $A\beta_{42}$-FITC (green), *H. pylori* OMVs-DiD (red), and incubation mixtures of $A\beta_{42}$-FITC and *H. pylori* OMVs-DiD at 37 °C for 24 h. Neurons were immunostained with antibody against MAP-2 (cyan). Nuclei were stained with Hoechst (blue). Scale bar, 50 μm. **I–K** Representative immunoblots and quantification for pre-synaptic protein synaptophysin (SYP) and post-synaptic protein PSD95 in neurons with different treatments ($n = 4$ for cell samples). Data shown as mean ± SEM, one-way ANOVA with Tukey test, $^{***}p < 0.001$.

synapses, severe cognitive deficit was observed in APP/PS1 mice injected with *H. pylori* OMVs when comparing to PBS- or *E. coli* OMVs-injected mice. These data indicate a specific pathogenic effect of *H. pylori* OMVs on APP/PS1 mice.

In APP/PS1 mice, increased Aβ production due to overexpression of mutated genes (APP Swedish mutation, PSEN1 deltaE9) plays a central role in causing AD-like pathogenesis and behavioral changes. Based on the observation that *H. pylori* OMVs promote amyloidosis, synaptic impairment and cognitive deficits in APP/PS1 mice, we speculate that *H. pylori* OMVs may act as a "trigger" or "catalyzer" of amyloidosis. To identify this hypothesis, we examined whether *H. pylori* OMVs aggravated Aβ pathology in vitro. ThT assay identified that *H. pylori* OMVs significantly accelerated Aβ aggregation compared with Aβ alone or *E. coli* OMVs. Under TEM, extensive amyloid fibers were observed at the end of incubation with *H. pylori* OMVs, and some *H. pylori* OMVs were found located on the surface of fibers, indicating that *H. pylori* OMVs may act as a catalytic surface for amyloid aggregation. Besides, we found that *H. pylori* OMVs significantly increased Aβ neurotoxicity in cultured primary neurons, which was consistent with animal experiments that *H. pylori* OMVs exacerbated Aβ pathology and synaptic impairment in APP/PS1 mice. According to amyloid cascade hypothesis, Aβ aggregates can initiate a cascade of events driving synapse loss, neuronal death, and cognitive impairment[4]. Although we also found *H. pylori* OMVs induced tau hyperphosphorylation and neuroinflammation, we proposed that the aggravated cognitive deficits and synaptic impairment in *H. pylori* OMVs-injected APP/PS1 mice was to a great extent caused by increased amyloidosis in the brain. Besides, we found that *H. pylori* OMVs-enhanced Aβ neurotoxicity mainly occurred at the postsynaptic sites, with postsynaptic PSD95 was reduced whereas presynaptic protein synaptophysin remained unchanged in *H. pylori* OMVs +Aβ treatment group. Numerous studies have shown that Aβ is toxic to synapses[46,53] and postsynaptic compartments of synapses are the prime targets of Aβ toxicity[54,55], where several putative receptors that mediate Aβ toxicity, such as the cellular prion protein, the α7 nicotinic acetylcholine receptor, NMDAR, AMPAR and mGluR5 are located[56]. In addition, there is a selective loss of PSD95, but not synaptophysin in hippocampus of hAPP AD mice as compared to their WT littermate controls[57]. Our data is consistent with these previous findings.

OMVs carry various bacterial molecules such as proteins, RNAs, DNAs and lipids, we next examined which component in *H. pylori* OMVs was involved in increasing Aβ neurotoxicity. Through specific removal of certain component in OMVs before the administration in cell experiments, we found that only depletion of lipids from *H. pylori* OMVs rescued neurotoxicity, indicating lipid components of *H. pylori* OMVs might be responsible for enhancing Aβ neurotoxicity. In addition, it was found that *H. pylori* OMVs after repeated freezing-thawing also enhanced Aβ neurotoxicity in primary neurons, suggesting that *H. pylori* OMVs-enhanced Aβ neurotoxicity probably does not depend on intact OMVs structure. To further identify which lipid in *H. pylori* OMVs is responsible for enhancing Aβ neurotoxicity, we performed quantitative lipidomics to reveal the differences in lipid profiles between *H. pylori* OMVs and *E. coli* OMVs. The results showed there was no difference in composition of lipid subclass between *H. pylori* OMVs and *E. coli* OMVs. However, the LPC levels, especially LPC15:0 and LPC 18:0 in *H. pylori* OMVs were significantly higher than those in *E. coli* OMVs. LPC is a bioactive polar phospholipid produced by hydrolysis of phosphatidylcholine (PC) by phospholipase A2 (PLA_2). Studies have shown changes in phospholipid metabolism in AD patients[58]. Increased PLA_2 activity was found in the brains of AD patients[59], and elevated LPC level was found in frontal lobe and cerebellum of elderly people with AD-type brain atrophy[60]. A large number of in vitro and in vivo studies have shown that LPC can lead to activation of microglia and neuroinflammation[61–63], which indicates that LPC may play an important role in the pathology of AD. In addition, previous studies also reported that LPC promoted $A\beta_{42}$ aggregation into fibers and enhanced Aβ-mediated neurotoxicity in vitro[64–66]. In our study, we found that LPC 18:0 which is abundant in *H. pylori* OMVs exerts the similar effects as *H. pylori* OMVs in accelerating Aβ aggregation and enhancing Aβ neurotoxicity both in vitro and in brain of APP/PS1 mice. In 6-month-old female APP/PS1 mice, *H. pylori* OMVs or LPC 18:0 injection into the hippocampus resulted in doubling of plaque area during 1 week. An investigation showed that the process of amyloid plaque growth followed a 'dock and lock' mechanism and further accretion of amyloid-β will occur once plaques are established[67]. Amyloid-β is rapidly accumulated into plaques, also as modeled in transgenic mice that are predisposed to form insoluble amyloid-β deposits[68]. Yan et al. used intravital multiphoton microscopy to study the growth of individual amyloid plaques of APP/PS1 mice and they found plaques exhibited significant growth over 7 d intervals in 6-month-old APP/PS1 mice[69]. Hefendehl et al. also used multiphoton imaging in vivo to follow the deposition of amyloid-β in APP/PS1 mice and they revealed an estimated rate of 35 newly formed plaques per cubic millimeter of neocortical volume per week at 4–5 months of age[70]. These studies, together with the observation in our study that *H. pylori* OMVs or LPC 18:0 accelerates plaque formation rapidly, strongly suggest that once entering the brain, *H. pylori* OMVs or its key pathologic component can promote amyloidosis potently. Our data indicate that *H. pylori* OMVs may accelerate Aβ aggregation and aggravate its neurotoxicity directly through LPC 18:0. The elevated LPC level found in AD brains may be also contributed by certain bacterial OMVs which is abundant of LPC and transferred into the brain from peripheral blood.

Recently, several studies reported that *H. pylori* OMVs exacerbate Aβ pathology and induce cognitive impairment via regulating glial cell activation[35,36]. Here we reveal a new mechanism focusing the direct effect of *H. pylori* OMVs on aggravating Aβ pathology through lipid components in OMVs. In fact, a series of findings indicate the role of membrane lipid in promoting Aβ aggregation and forming β-sheet structure. For example, lipid membranes containing cholesterol could promote $A\beta_{42}$ aggregation by enhancing its primary nucleation rate via a heterogeneous nucleation pathway[71]. Aβ selectively recognizes gangliosides GM1 on the membrane surface, adopts an altered conformation by binding to GM1 and acts as a template for accelerating Aβ assembly[72]. Besides, compelling data suggest that the phospholipid phosphatidylserine is very likely to be the elusive membrane surface receptor site for Aβ binding[73,74], and the ability of Aβ to associate with membranes and form channels is enhanced by exposure of phosphatidylserine on the cell surface[75]. Although most of these studies

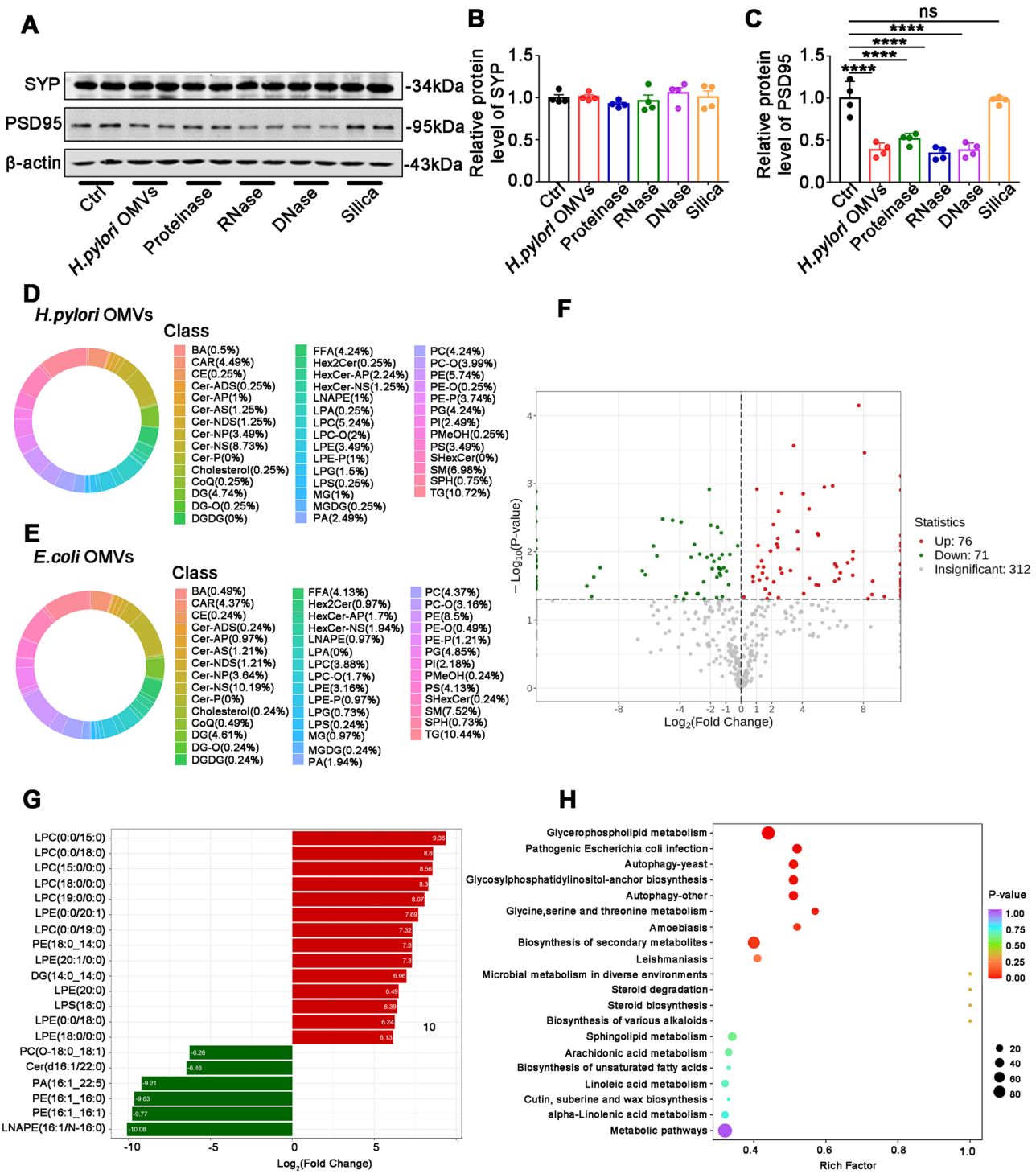

Fig. 4 | Lipid components in *H. pylori* OMV contribute to the enhancement of Aβ neurotoxicity. **A**–**C** Representative immunoblots and quantification for SYP and PSD95 in neurons treated with different *H. pylori* OMVs-incubated Aβ aggregates. Before incubated with Aβ, *H. pylori* OMVs were removed of proteins, RNAs, DNAs, or lipids, respectively ($n = 4$ for cell samples). Data shown as mean ± SEM, one-way ANOVA with Tukey test, $^{****}p < 0.0001$. **D** Circular diagram of lipid subclass composition in *H. pylori* OMVs. **E** Circular diagram of lipid subclass composition in *E. coli* OMVs. **F** Volcano plot showing differential lipids between *H. pylori* and *E. coli* OMVs. **G** The top fold change (FC)-20 differential lipids between *H. pylori* OMVs and *E. coli* OMVs. **H** KEGG enrichment analysis for differential lipids between *H. pylori* OMVs and *E. coli* OMVs. The top-20 enriched lipid pathways (with p-values) are displayed.

attempted to disclose the mechanisms of Aβ binding to cell membrane, especially neuronal cell membrane, these data shed light on the role of bacteria-originated membrane lipid in promoting Aβ aggregation and cell toxicity. In our study, the detailed mechanisms of LPC binding to Aβ and affecting fibril formation needs to be further investigated. It is also of great significance to explore whether this phenomenon is common to OMVs from other bacteria that have been reported to participated in the development of AD. Besides, recently several studies have shown that enteric bacteria such as *E. coli* and *Salmonella* produce fibrillar structures that are analogous to Aβ amyloids, called functional amyloids, which have also been reported to have a role in the pathogenesis of Alzheimer's and Parkinson's disease[76–78]. For example, CsgA curli amyloids secreted by *E. coli* was

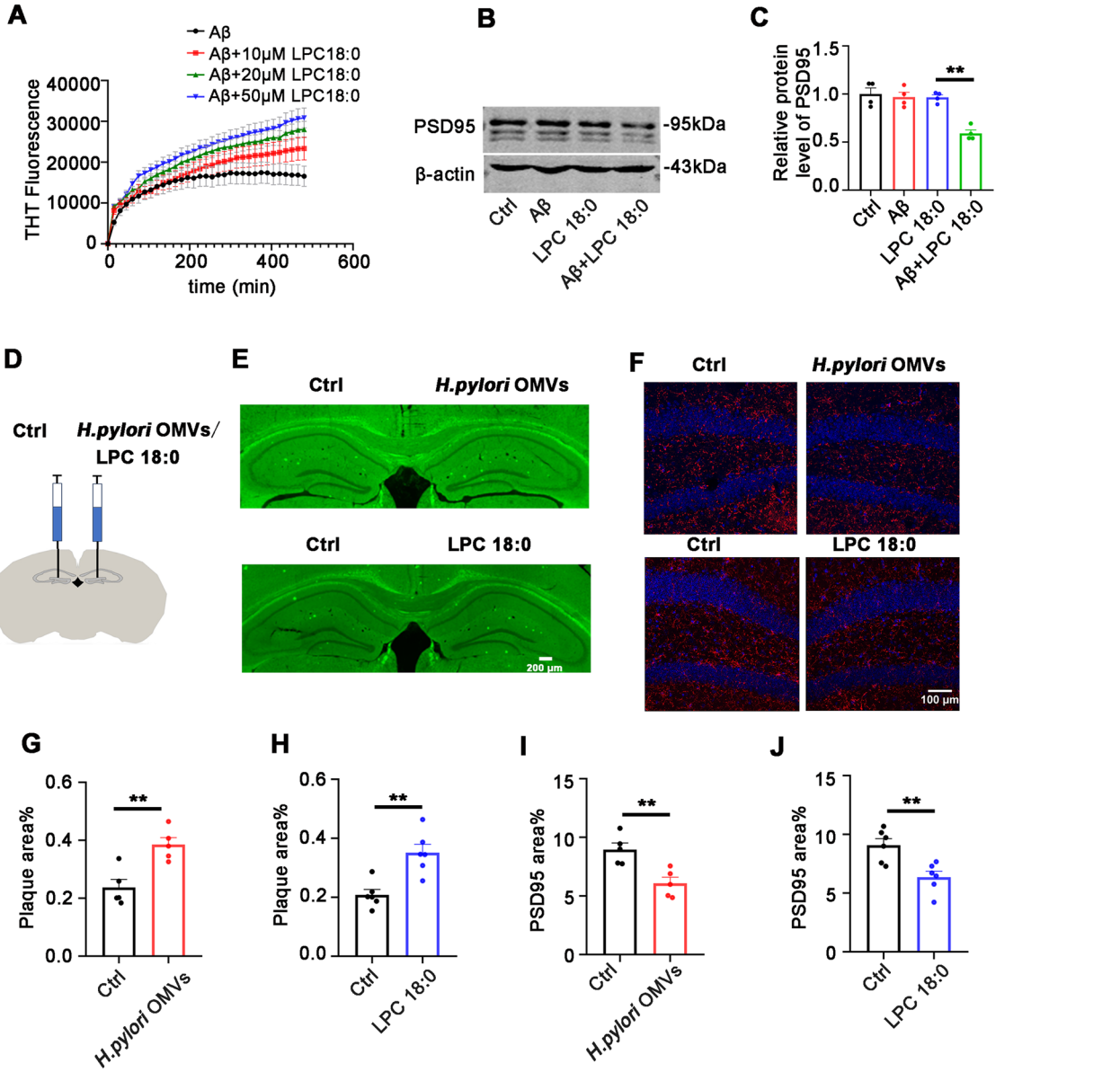

Fig. 5 | LPC 18:0 in *H. pylori* OMVs accelerates Aβ aggregation and enhances Aβ neurotoxicity in vitro and in brain of APP/PS1 mice. A Aggregation kinetics of $A\beta_{42}$ incubated alone or with 10 μM (5.236 μg/ml), 20 μM (10.473 μg/ml) and 50 μM (26.184 μg/ml) of LPC 18:0 monitored by ThT assay. The averaged data from three replicates and standard deviations are plotted. **B**, **C** Cultured primary neurons were treated with PBS, $A\beta_{42}$ aggregates alone, LPC 18:0 alone, LPC 18:0-incubated $A\beta_{42}$ aggregates at 37 °C for 24 h. Representative immunoblots and quantification for synaptic protein PSD95 in neurons with different treatments ($n = 4$ for cell samples). Data shown as mean ± SEM, one-way ANOVA with Tukey test, $^{**}p < 0.01$. **D** Schematic of the site of intracerebrally hippocampus injections (posterior 1.9 mm, lateral ± 1.1 mm from bregma, ventral −2.0 mm from the skull). **E** Representative images of Aβ plaque staining with THS (Green) in the hippocampus of APP/PS1 mice intracerebrally injected with normal saline, *H. pylori* OMVs or LPC 18:0. Scale bar, 200 μm. **F** Representative immunofluorescent staining images for PSD95 (Red) in DG of the hippocampus of APP/PS1 mice intracerebrally injected with normal saline, *H. pylori* OMVs or LPC 18:0. Nuclei were stained with Hoechst (Blue). Scale bar, 100 μm. **G**, **H** Quantification of THS-positive plaques in the hippocampus of APP/PS1 mice (3 mice per group and 2–3 slices per mouse). Data shown as mean ± SEM, two-tailed Student's *t* test, $^{**}p < 0.01$. **I**, **J** Quantification of PSD95 fluorescence signaling in DG of the hippocampus of APP/PS1 mice (3 mice per group and 2–3 slices per mouse); data shown as mean ± SEM, two-tailed Student's *t* test, $^{**}p < 0.01$.

reported to accelerate α-synuclein aggregation in vitro and induce PD symptoms in mice[78]. In addition, human $A\beta_{42}$ can specifically target and dissolve microbial amyloids. Thus, it's interesting to explore possible mechanism that links peripheral bacterial infection and disorders in central nerves system. At last, we showed *H. pylori* OMVs may accelerate Aβ aggregation through lipid LPC, however, other contents in OMVs which involved in Aβ aggregation may also exist, which needs further study.

Aggregated Aβ has the ability to insert into membranes and form transmembrane pores which allow the influx of Ca2+ [79], the latter, plays a key role in mediating the cytotoxicity of Aβ. Thus, the *H. pylori* OMVs-enhanced Aβ toxicity is possibly induced by the intracellular calcium overload resulted from increased Aβ aggregation. In our study, both incubation mixture of *H. pylori* OMVs with Aβ and LPC 18:0 with Aβ significantly increased intracellular Ca^{2+} level and reduced the level of synaptic protein PSD95 in primary neurons. With the removal of extracellular Ca^{2+}, the decrease of synaptic protein PSD95 was reversed, indicating that *H. pylori* OMVs-enhanced Aβ toxicity is mediated by Ca^{2+} influx.

In conclusion, we demonstrate that *H. pylori* OMVs accelerate Aβ aggregation and enhance Aβ toxicity directly through lipid, thus exacerbating AD pathology and cognitive impairment. Our data highlight the role of OMVs secreted by bacteria in bacteria–host interactions and reveal a convergence between *H. pylori* infection and amyloid pathologies in AD.

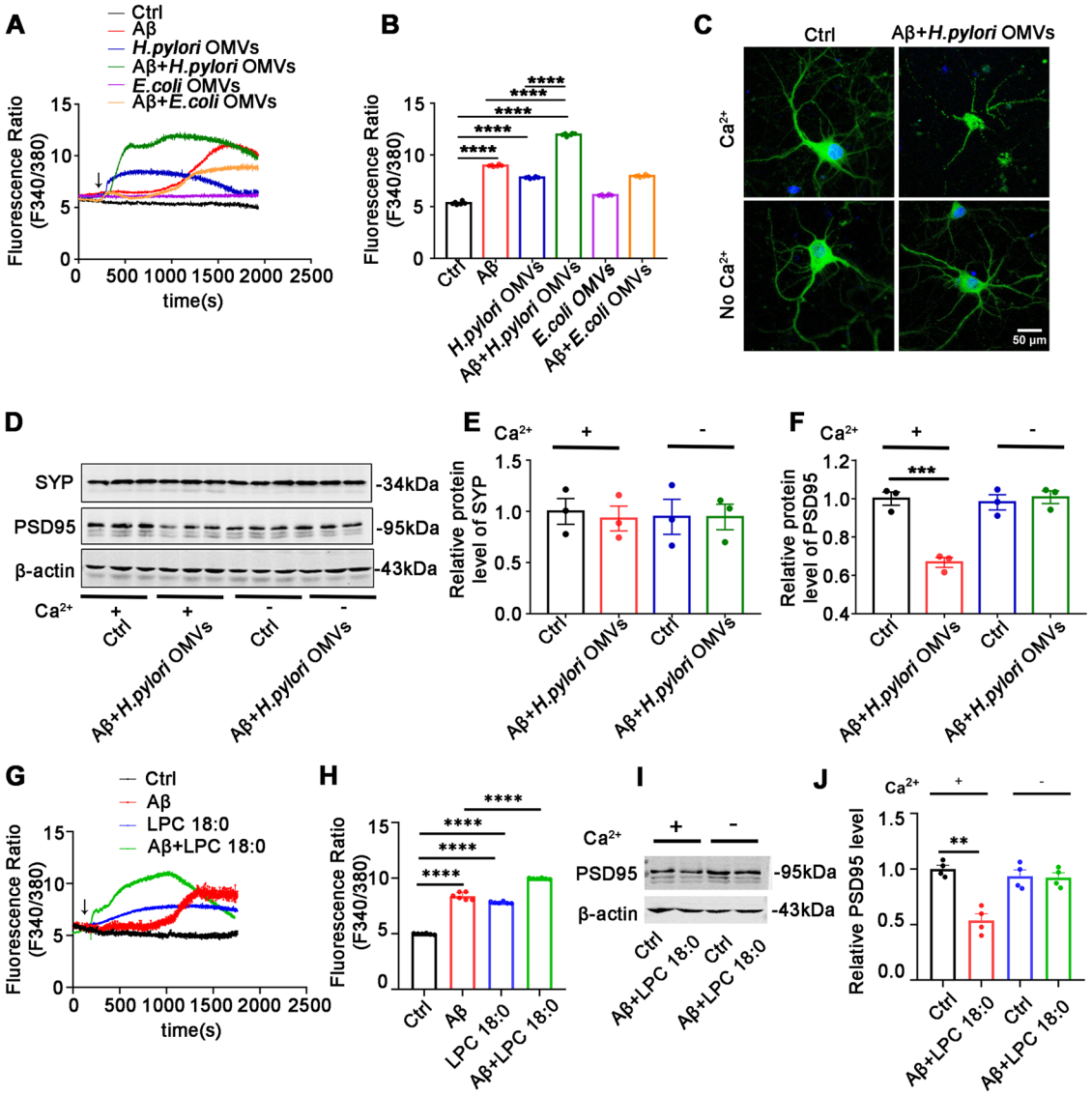

Fig. 6 | *H. pylori* OMVs and LPC 18:0-enhanced Aβ toxicity is mediated by Ca^{2+}. **A** Graph showing the effects of different treatments, including $Aβ_{42}$ aggregates alone, *H. pylori* OMVs alone, *H. pylori* OMVs-incubated $Aβ_{42}$ aggregates, *E. coli* OMVs alone, and *E. coli* OMVs-incubated $Aβ_{42}$ aggregates on levels of intracellular Ca^{2+}. Arrow indicates the beginning of the treatment application. **B** Intracellular Ca^{2+} levels in primary neurons measured after 20 minutes of treatment. $n = 6$ cells. Data shown as mean ± SEM, one-way ANOVA with Tukey test, $^{****}p < 0.0001$. **C** Morphologic changes of neurons after 24 hours of treatment with *H. pylori* OMVs-incubated Aβ aggregates in the presence or absence of extracellular Ca^{2+}. Scale bar, 50 μm. **D**–**F** Representative immunoblots and quantification for synaptic proteins, including SYP and PSD95 in neurons treated with *H. pylori* OMVs-incubated Aβ aggregates in the presence or absence of extracellular Ca^{2+}. $n = 3$ for cell samples. Data shown as mean ± SEM, one-way ANOVA with Tukey test, $^{***}p < 0.001$. **G** Graph showing the effects of different treatments including $Aβ_{42}$ aggregates alone, LPC 18:0 alone, LPC 18:0-incubated $Aβ_{42}$ aggregates on levels of intracellular Ca^{2+}. Arrow indicates the beginning of the treatment application. **H** Intracellular Ca^{2+} levels in primary neurons measured after 20 minutes of treatment. $n = 6$ cells. Data are shown as mean ± SEM, one-way ANOVA with Tukey test, $^{****}p < 0.0001$. **I**, **J** Representative immunoblots and quantification for synaptic protein PSD95 in neurons treated with *H. pylori* OMVs-incubated Aβ aggregates in the presence or absence of extracellular Ca^{2+}. $n = 4$ for cell samples. Data are shown as mean ± SEM, one-way ANOVA with Tukey test, $^{**}p < 0.01$.

Materials and methods

Bacterial strains and culture

Bacterial strains used in this study: *H. pylori* strain 49503 and *E. coli* strain 25922 were from American Type Culture Collection (Manassas, VA, USA). *H. pylori* were grown on blood agar plates of brain heart infusion agar supplemented with 10% sheep blood at 37 °C for 72 h during the late stationary phase in a microaerophilic environment of 5% O_2, 10% CO_2, and 85% N_2. *E. coli* were cultured in Luria-Bertani broth at 37 °C for 24 h in an aerobic environment.

Isolation, characterization, and fluorescence labeling of OMVs

Isolation of *H. pylori* OMVs and *E. coli* OMVs was performed according to Jung et al. with the following modifications[80]: *H. pylori* were grown on blood agar plates for 72 h, then harvested in PBS and centrifuged twice for 30 min at 4000 × *g* at 4 °C to remove cells and debris. *E. coli* were grown in Luria-Bertani broth for 24 h and centrifuged twice for 30 min at 4000 × *g* at 4 °C. The supernatant was filtered through a 0.22 μm cellulose acetate filter and centrifugated twice for 2 h at 120,000 × *g* at 4 °C in a Type SW41Ti rotor using an L-80XP μLtracentrifuge (Beckman Coulter, USA). The pellet containing vesicles was resuspended in PBS and analyzed using BCA Protein Assay kit. The morphology of OMVs was examined by TEM. The size distribution and concentration of the OMVs were determined by nanoparticle tracking analysis (NTA) using a ZetaView PMX 110 analyzer (Particle Metrix, Meerbusch, Germany) equipped with a ZetaView 8.05.14 SP7 software. For fluorescence labeling, OMVs were resuspended in sterile PBS and incubated with 1 μM red fluorescence dye DiD (Biotium, USA) for

15 min at 37 °C. DiD-OMVs were then washed in sterile PBS and centrifugated twice for 2 h at 120,000 × *g* at 4 °C to remove free DiD and other impurities such as lipoproteins. The control was prepared by DiD incubation with PBS (DiD-ctrl), which was washed same as the DiD-OMVs preparation.

Animals and treatment

C57BL/6 mice were purchased from HFK Bioscience (Beijing, China). APP/PS1 mice were from the Jackson Laboratory (Bar Harbor, ME, USA). Mice were housed (4–5 per cage) under standard laboratory conditions (temperature: 23 ± 1 °C, humidity: 55 ± 5%), with a 12 h alternating light/dark cycle and unrestricted access to food and water. All animal experiments were approved by the Animal Care and Use Committee of Huazhong University of Science and Technology. To determine the effect of OMVs on Aβ pathology, 3-month-old C57BL/6 J mice and APP/PS1 mice received intraperitoneal injection of *H. pylori* OMVs, *E. coli* OMVs or an equivalent volume of PBS every other day for 6 months (10 μg of total protein of OMVs in 0.1 ml PBS/per mice) and were sacrificed at the end of behavioral tests. To detect whether OMVs enter the brain, APP/PS1 mice at the age of 9 months were intraperitoneally injected with 10 μg of DiD-labeled OMVs and euthanized after 48 h. To examine the direct effect of *H. pylori* OMVs and LPC 18:0 on Aβ pathology, 6-month-old APP/PS1 mice were anesthetized with 1% pentobarbital sodium (35 mg/kg), and then fixed in a stereotaxic instrument (RWD, Shenzhen, China). The scalp was sterilized with iodophors and incised along the skull midline. Two holes were drilled bilaterally at posterior 1.9 mm, lateral ± 1.1 mm from begma. 2 μl of solution containing *H. pylori* OMVs (5 μg of total protein of OMVs) and LPC 18:0 (50 μM) was injected into right hippocampal dentate gyrus (DG) (ventral -2.0 from the skull) respectively, and same volume of normal saline was injected into left hippocampal DG as control. The solutions were injected at 0.1 μl/min, and the needle was left in place for 5 min. Lysophosphatidylcholine (LPC) was purchased from Avanti Polar Lipids (Alabaster, AL) and dissolved in normal saline. Mice were perfused with 0.9% saline and 4% PFA one week after injection. The brains were removed and sectioned for immunostaining.

Morris water maze

The MWM was performed in a circular pool filled with opaque water set at 25 °C. Training consisted of 6 days of four swim trials (60 s per trial) per day with different quadrant starting positions for each trial. One day after the last training, the mice were given a probe test. During the probe test, mice were allowed to swim for 60 s without the platform in the pool. After establishing robust spatial preference for the platform location, at day 10, mice started a new training session, where the platform was located in the opposite position to start reversal learning. The whole process was recorded and analyzed by a video tracking system (Techman Software, Chengdu, China). The escape latency in training and during the probe tests, time spent in the target quadrant, the numbers of crossing the location of the platform, and swim speed (mm/s) were analyzed.

Contextual discrimination test

Contextual discrimination task was performed according to the method described by Yang et al.[81].

Preparation of brain slices

Mice were deeply anesthetized by intraperitoneal injection with 1% pentobarbital sodium (35 mg/kg) and perfused from the left ventricle with ice-cold 0.9% saline, and brains were quickly removed, fixed in 4% paraformaldehyde at 4 °C for 12 h, and then dehydrated in 20% and 30% sucrose solutions for frozen section. Brain coronal sections of 40 μm thickness were sliced in a cryostat microtome (CM1900, Leica).

Immunostaining

Primary neurons on glass coverslips were fixed with 4% paraformaldehyde for 10 min, then fixed neurons or free-floating brain sections were washed with PBS, blocked with 3% BSA in PBS containing 0.5% Triton X-100 for 1 h, and then probed with the primary antibodies: 4G8 (1:200, SIG-39220, BioLegend), MAP-2 (1:200, 4542, Cell Signaling, USA), Iba-1 (1:200, 091-19741, Wako) at 4 °C for 24 h. After washed in PBS, brain slices and cells were incubated with secondary antibodies at 37 °C for 2 h. The secondary antibody used for 4G8 is goat anti-mouse Alexa Fluor 488 (115-545-003, 1:300, Jackson ImmunoResearch, USA), for MAP-2 and Iba-1 is goat anti-rabbit Alexa Fluor 594 (111-515-047, 1:300, Jackson ImmunoResearch, USA). The nuclei were stained with Hoechst at concentration of 10 μg/ml. Fluorescence images were photographed by two-photon laser-scanning confocal microscope (LSM 780, Carl Zeiss, Jena, Germany).

Thioflavin-S staining

Thioflavin-S (Cat #T1892, Sigma-Aldrich, USA) staining was performed as followed: free-floating brain sections were incubated with 0.3% Thioflavin-S (dissolved in 50% ethanol) at room temperature for 15 min, then were decolorized in 50% ethanol for 3 × 5 min, washed in PBS and finally mounted with a buffer containing 50% PBS and 50% glycerol. Images were taken by a virtual slide Microscope (SV120, Olympus).

Golgi staining

The left hemispheres were dissected and immersed in the Golgi-Cox solution (5% potassium dichromate, 5% mercuric chloride and 5% potassium chromate) for 30 days. Then, the brains were transferred to a 30% sucrose solution and stored in the dark at 4 °C. Coronal mouse brains sections (100 μm) were sliced using Vibratome (VT1000S, Leica) and transferred onto 1% gelatin-coated slides. The slices were then treated with ammonium hydroxide for 10 minutes, followed by incubation in an increasing grade of ethanol (50%, 75%, 95% and 100%), then in xylene for 15 minutes, and finally mounted in permount TM mounting medium. Stained sections were imaged using a 100x oil immersion objective of microscope (Nikon, 90i, Tokyo, Japan).

Enzyme-linked immunosorbent assay

Left hippocampus and cortex were isolated on ice and homogenized with PBS containing PMSF and protease inhibitor cocktail (Yeasen, China), and then centrifuged for 15 min at 4 °C, 12,000 rpm. The supernatants were collected for the detection of PBS-soluble fraction Aβ and pro-inflammatory cytokine IL-6, and the pellets were dissolved with 70% formic acid for 15 min for the detection of insoluble Aβ. IL-6, $A\beta_{40}$ and $A\beta_{42}$ were measured using ELISA kits from Elabscience (Cat# E-EL-M0044c, E-EL-H0542c, and E-EL-H0543c), respectively. All procedures followed the manufacturer's instructions.

Western blotting

Right hippocampus and cortex were isolated and homogenized in 10 volumes (ml/g wet tissue) RIPA lysis buffer (Beyotime, China) containing PMSF and protease inhibitor cocktail (Yeasen, China), and then centrifuged for 15 min at 4 °C, 12,000 rpm. The supernatants were collected and protein concentration was determined by BCA protein assay kit. Protein samples were loaded and separated by sodium dodecyl sulfate-polyacrylamide (SDS-PAGE) gels electrophoresis and transferred to nitrocellulose blotting membranes (GE Healthcare Life science, Germany). The membranes were blocked with 5% BSA, incubated with primary and IRDye-conjugated secondary antibodies in turn. Primary antibodies are listed in Table S1. All Western blotting signals were scanned using the Odyssey Infrared Imaging System (Li-cor Biosciences, Lincoln, NE, USA), and the protein bands were quantified and analyzes using Image J software.

Assay of Aβ aggregation

Human $A\beta_{42}$ peptides was purchased from China Peptides (Shanghai, China). Thioflavin T (ThT, Cat #T3516, Sigma-Aldrich, USA) fluorescence assay was performed as follows: $A\beta_{42}$ monomer solutions (dissolved in 0.02% ammonia solution at 25 μM) were incubated with 10 μg/ml of *H. pylori* OMVs and *E. coli* OMVs in TBS at 37 °C for 8 h. Besides, $A\beta_{42}$

monomer solutions (25 μM) were incubated with 0.5, 1 or 5 μg/ml of *H. pylori* OMVs to examine dose-dependent effect on Aβ aggregation. To examine the effect of LPC 18:0 on Aβ aggregation, $Aβ_{42}$ monomer solutions (25 μM) were incubated with 10, 20 or 50 μM LPC 18:0 in TBS at 37 °C for 8 h. The samples were incubated in a 96-well opaque microtiter plate and monitored by a spectrometer (Synergy H1; BioTek). The optimum fluorescence intensities of amyloid fibrils were monitored at an excitation wavelength of 446 nm and an emission wavelength of 490 nm, with the reaction mixtures containing 5 μM ThT solution. Data were plotted and analyzed in GraphPad Prism 7.0.

Transmission electron microscopy

Ten microliters isolated OMVs or sample solution from ThT assay were placed on a carbon-coated copper grid (Beijing Zhongjingkeyi Technology Co., Ltd, China) for 1 min. The grids were blotted, washed with droplets of μLtrapure water, and negatively stained for 1 min by adding an equal volume of 2% (w/v) uranyl acetate. Images were captured using Hitachi TEM system (Japan) operating at 80.0 kV.

Primary neuron culture and treatments

Primary neurons were prepared from the isolated cerebral cortices of Sprague Dawley rat brains on embryonic day 18. To examine the effect of OMVs and LPC on Aβ-induced neurotoxicity, $Aβ_{42}$ was pre-incubated alone or with OMVs and LPC at 37 °C for 8 h in neurobasal medium. The incubation mixtures were subsequently applied to the primary neurons and incubated for 24 h. The final concentration of $Aβ_{42}$ was 1 μM, OMVs was 1 μg/ml, and LPC 18:0 was 50 μM, neurons treated with PBS were used as control in all above experiments. In neurons treated with $Aβ_{42}$-FITC, the concentration of FITC was 0.58 μM. For exploring the role of Ca^{2+} in H. pylori enhanced Aβ neurotoxicity, pre-incubation mixtures of $Aβ_{42}$ and *H. pylori* OMVs were administered to primary neurons in the presence or absence of extracellular calcium for 24 h at 37 °C.

LDH cytotoxicity assay

The pre-incubated mixtures of $Aβ_{42}$ and OMVs (or LPC 18:0) were applied to the primary neurons that had been plated on 6-well plates and incubated for 24 h. The cytotoxicity was determined using LDH cytotoxicity assay kit (C20300, Thermo Fisher).

Elimination of proteins, RNAs, DNAs, or lipids from OMVs

OMVs were resuspended in PBS for the following processing: OMVs underwent five freeze-thaw cycles (−80°C ~ 37°C) first to release the components in the vesicles completely. (1) To remove proteins, OMVs components were treated with proteinase (Sigma, 0.5 mg/mL, 58°C) for 2 h to degrade proteins, followed by 20 min boiling to inactivated proteinase. (2) To remove RNAs, OMVs components were treated with RNase A (Takara, 10 μg/ml, 37°C) for 1 h, followed by 1 h incubation with RNase A inhibitor (Takara, 2000 units/mL, 37°C) to inactivate RNase A. (3) To remove DNAs, OMVs components were treated with DNase (Promega, 10 units/mL, 37 °C) for 0.5 h, followed by 0.5 h incubation with stop solution to inactivate DNase. (4) To remove lipids from OMVs components, fumed silica (Sigma, S5130, 20 mg/mL) was added, followed by mixing overnight, centrifuging for 15 min at 4 °C, 12,000 rpm, and sterile filtration to harvest a medium free of lipids.

Lipidomic analysis

(1) Sample preparation: OMVs suspension was added with 500 μL mixture (include methanol, MTBE and internal standard mixture). After whirled for 15 min, the mixture was centrifuged at 12,000 rpm for 10 min at 4°C. Supernatant was concentrated and the power was dissolved with 200 μL reconstituted solution, then stored in −80 °C. (2) UPLC-MS/MS analysis was carried out according to previous studies described[82,83]. Briefly, chromatographic separation was achieved on an ExionLC AD UPLC system (Sciex) with the Thermo Accucore™C30 column (2.6 μm, 2.1 mm × 100 mm i.d.). Gradient program was t = 0 min: A/B (80:20, V/V); t = 2.0 min: A/B (70:30, V/V); *t* = 4 min: A/B (40:60, V/V); t = 9 min: A/B (15:85, V/V), t = 14 min: A/B (10:90, V/V); t = 15.5 min: A/B (5:95, V/V); t = 17.3 min: A/B (5:95, V/V); t = 17.5 min: A/B (80:20, V/V); t = 20 min: A/B (80:20, V/V). Acquisition of MS data was undertaken on a QTRAP® 6500 + LC-MS/MS system (Sciex) in MRM mode with the following parameters: positive ion spray voltage, 5500 V; negative ions pray voltage, −4500 V; source temperature, 500°C; ion source gas 1, 45 psi; ion source gas 2, 55 psi; curtain gas, 35 psi. (3) Qualitative and Quantitative analysis: The MWDB (metware database) was constructed based on the standard materials to qualitatively analyze the data detected by mass spectrometry. The multiple reaction monitoring (MRM) mode of triple quadrupole mass spectrometry was applied for the quantification of analytes.

Intracellular calcium imaging

Neurons grown on PDL-coated glass coverslips were incubated with Fura-2 AM (3 μM, 108964-32-5, Dojindo, Japan) for 30 min at 37°C. The calcium imaging experiments were carried out using the FLUOVIEW V.5.0 Software. The excitation wavelengths were set at 340 nm and 380 nm, and the emission wavelengths at 510 nm. Fluorescent signal from regions of interest (ROI) in different neurons was collected at 1- to 2-second intervals during a continuous 30-minute period, using an Olympus inverted confocal microscope (IX71, Japan) associated with FLUOVIEW V.5.0 Software.

Statistics and reproducibility

Student's *t* test and one-way and two-way analysis of variance (ANOVA) statistical analyses were performed using GraphPad Prism 8.0. Analysis of ANOVA with post hoc test was used when comparing more than two groups, whereas unpaired *t* test was used when comparing only two groups. For all quantifications, the data are expressed as the mean ± SEM. Significance was concluded when $p < 0.05$, indicated by $^{*}p < 0.05$, $^{**}p < 0.01$, $^{***}p < 0.001$, and $^{****}p < 0.0001$.

Reporting summary

Further information on research design is available in the Nature Portfolio Reporting Summary linked to this article.

Data availability

All data generated or analyzed during this study are included in this published article and its supplementary information files. All data are available from the corresponding authors upon reasonable request.

Received: 24 April 2024; Accepted: 22 October 2024;
Published online: 09 November 2024

References

1. Mattson, M. P. Pathways towards and away from Alzheimer's disease. *Nature* **430**, 631–639 (2004).
2. Qian, X., Hamad, B. & Dias-Lalcaca, G. The Alzheimer disease market. *Nat. Rev. Drug Discov.* **14**, 675–676 (2015).
3. Bloom, G. S. Amyloid-beta and tau: the trigger and bullet in Alzheimer disease pathogenesis. *JAMA Neurol.* **71**, 505–508 (2014).
4. Korczyn, A. D. The amyloid cascade hypothesis. *Alzheimers Dement.* **4**, 176–178 (2008).
5. Ross, C. A. & Poirier, M. A. Protein aggregation and neurodegenerative disease. *Nat. Med*. **10**, S10–S17 (2004).
6. Hardy, J. & Selkoe, D. J. The amyloid hypothesis of Alzheimer's disease: progress and problems on the road to therapeutics. *Science* **297**, 353–356 (2002).
7. Abbott, A. Are infections seeding some cases of Alzheimer's disease? *Nature* **587**, 22–25 (2020).

8. Itzhaki, R. F., Golde, T. E., Heneka, M. T. & Readhead, B. Do infections have a role in the pathogenesis of Alzheimer disease? *Nat. Rev. Neurol.* **16**, 193–197 (2020).
9. Panza, F., Lozupone, M., Solfrizzi, V., Watling, M. & Imbimbo, B. P. Time to test antibacterial therapy in Alzheimer's disease. *Brain* **142**, 2905–2929 (2019).
10. Ashraf, G. M. et al. The possibility of an infectious etiology of Alzheimer disease. *Mol. Neurobiol.* **56**, 4479–4491 (2019).
11. Fulop, T., Itzhaki, R. F., Balin, B. J., Miklossy, J. & Barron, A. E. Role of microbes in the development of Alzheimer's disease: state of the art - an international symposium presented at the 2017 IAGG Congress in San Francisco. *Front Genet*. **9**, 362 (2018).
12. Honjo, K., van Reekum, R. & Verhoeff, N. P. Alzheimer's disease and infection: do infectious agents contribute to progression of Alzheimer's disease? *Alzheimers Dement.* **5**, 348–360 (2009).
13. Hooi, J. K. Y. et al. Global prevalence of helicobacter pylori infection: systematic review and meta-analysis. *Gastroenterology* **153**, 420–429 (2017).
14. Doulberis M. et al. Review: impact of Helicobacter pylori on Alzheimer's disease: what do we know so far? *Helicobacter* **23**, e12454 (2018).
15. Franceschi, F. et al. Microbes and Alzheimer' disease: lessons from H. pylori and GUT microbiota. *Eur. Rev. Med. Pharm. Sci.* **23**, 426–430 (2019).
16. Kountouras, J. et al. Impact of Helicobacter pylori and/or Helicobacter pylori-related metabolic syndrome on incidence of all-cause and Alzheimer's dementia. *Alzheimers Dement.* **15**, 723–725 (2019).
17. Beydoun, M. A., Beydoun, H. A., Elbejjani, M., Dore, G. A. & Zonderman, A. B. Helicobacter pylori seropositivity and its association with incident all-cause and Alzheimer's disease dementia in large national surveys. *Alzheimers Dement.* **14**, 1148–1158 (2018).
18. Kountouras, J. et al. Relationship between Helicobacter pylori infection and Alzheimer disease. *Neurology* **66**, 938–940 (2006).
19. Kountouras, J. et al. Eradication of Helicobacter pylori may be beneficial in the management of Alzheimer's disease. *J. Neurol.* **256**, 758–767 (2009).
20. Kountouras, J. et al. Helicobacter pylori-related ApoE 4 polymorphism may be associated with dysphagic symptoms in older adults. *Dis. Esophagus* **29**, 842 (2016).
21. Contaldi, F. et al. The hypothesis that Helicobacter pylori predisposes to Alzheimer's disease is biologically plausible. *Sci. Rep.* **7**, 7817 (2017).
22. Wang, X. L. et al. Helicobacter pylori filtrate impairs spatial learning and memory in rats and increases beta-amyloid by enhancing expression of presenilin-2. *Front. Aging Neurosci.* **6**, 66 (2014).
23. Wang, X. L. et al. Helicobacter pylori filtrate induces Alzheimer-like tau hyperphosphorylation by activating glycogen synthase kinase-3beta. *J. Alzheimers Dis.* **43**, 153–165 (2015).
24. Toyofuku, M., Nomura, N. & Eberl, L. Types and origins of bacterial membrane vesicles. *Nat. Rev. Microbiol.* **17**, 13–24 (2019).
25. Schwechheimer, C. & Kuehn, M. J. Outer-membrane vesicles from Gram-negative bacteria: biogenesis and functions. *Nat. Rev. Microbiol.* **13**, 605–619 (2015).
26. Roier, S. et al. A novel mechanism for the biogenesis of outer membrane vesicles in Gram-negative bacteria. *Nat. Commun.* **7**, 10515 (2016).
27. Kulkarni, H. M. & Jagannadham, M. V. Biogenesis and multifaceted roles of outer membrane vesicles from Gram-negative bacteria. *Microbiology* **160**, 2109–2121 (2014).
28. Sartorio, M. G., Pardue, E. J., Feldman, M. F. & Haurat, M. F. Bacterial outer membrane vesicles: from discovery to applications. *Annu. Rev. Microbiol.* **75**, 609–630 (2021).
29. Park, A. M. & Tsunoda, I. Helicobacter pylori infection in the stomach induces neuroinflammation: the potential roles of bacterial outer membrane vesicles in an animal model of Alzheimer's disease. *Inflamm. Regen.* **42**, 39 (2022).
30. Wei, S. et al. Outer membrane vesicles enhance tau phosphorylation and contribute to cognitive impairment. *J. Cell Physiol.* **235**, 4843–4855 (2020).
31. Yoshida K. et al. Porphyromonas gingivalis outer membrane vesicles in cerebral ventricles activate microglia in mice. *Oral Dis*. **29**, 3688–3697 (2022).
32. Gong, T. et al. Outer membrane vesicles of Porphyromonas gingivalis trigger NLRP3 inflammasome and induce neuroinflammation, tau phosphorylation, and memory dysfunction in mice. *Front. Cell Infect. Microbiol.* **12**, 925435 (2022).
33. Ha, J. Y., Choi, S. Y., Lee, J. H., Hong, S. H. & Lee, H. J. Delivery of periodontopathogenic extracellular vesicles to brain monocytes and microglial IL-6 promotion by RNA cargo. *Front. Mol. Biosci.* **7**, 596366 (2020).
34. Bittel, M. et al. Visualizing transfer of microbial biomolecules by outer membrane vesicles in microbe-host-communication in vivo. *J. Extracell. Vesicles* **10**, e12159 (2021).
35. Xie, J. et al. Helicobacter pylori-derived outer membrane vesicles contribute to Alzheimer's disease pathogenesis via C3-C3aR signalling. *J. Extracell. Vesicles* **12**, e12306 (2023).
36. Palacios, E. et al. Helicobacter pylori outer membrane vesicles induce astrocyte reactivity through nuclear factor-kappaappa B activation and cause neuronal damage in vivo in a murine model. *J. Neuroinflamm.* **20**, 66 (2023).
37. Suzuki, T. & Nakaya, T. Regulation of amyloid beta-protein precursor by phosphorylation and protein interactions. *J. Biol. Chem.* **283**, 29633–29637 (2008).
38. Jucker, M. & Walker, L. C. Alzheimer's disease: From immunotherapy to immunoprevention. *Cell* **186**, 4260–4270 (2023).
39. Biancalana, M. & Koide, S. Molecular mechanism of Thioflavin-T binding to amyloid fibrils. *Biochim. Biophys. Acta* **1804**, 1405–1412 (2010).
40. Williams, T. L., Day, I. J. & Serpell, L. C. The effect of Alzheimer's Abeta aggregation state on the permeation of biomimetic lipid vesicles. *Langmuir* **26**, 17260–17268 (2010).
41. Linse, S. et al. Nucleation of protein fibrillation by nanoparticles. *Proc. Natl Acad. Sci. USA* **104**, 8691–8696 (2007).
42. Mahmoudi, M., Kalhor, H. R., Laurent, S. & Lynch, I. Protein fibrillation and nanoparticle interactions: opportunities and challenges. *Nanoscale* **5**, 2570–2588 (2013).
43. Buell, A. K. The nucleation of protein aggregates - from crystals to amyloid fibrils. *Int Rev. Cell Mol. Biol.* **329**, 187–226 (2017).
44. Brovkovych, V., Aldrich, A., Li, N., Atilla-Gokcumen, G. E. & Frasor, J. Removal of serum lipids and lipid-derived metabolites to investigate breast cancer cell biology. *Proteomics* **19**, e1800370 (2019).
45. Ferraz, T. P., Fiuza, M. C., Dos Santos, M. L., Pontes De Carvalho, L. & Soares, N. M. Comparison of six methods for the extraction of lipids from serum in terms of effectiveness and protein preservation. *J. Biochem. Biophys. Methods* **58**, 187–193 (2004).
46. Spires-Jones, T. L. & Hyman, B. T. The intersection of amyloid beta and tau at synapses in Alzheimer's disease. *Neuron* **82**, 756–771 (2014).
47. Zou, J. et al. A differential role of macrophage TRPM2 channels in Ca(2)(+) signaling and cell death in early responses to H(2)O(2). *Am. J. Physiol. Cell Physiol.* **305**, C61–C69 (2013).
48. Montagne, A. et al. Blood-brain barrier breakdown in the aging human hippocampus. *Neuron* **85**, 296–302 (2015).
49. Bielaszewska, M. et al. Host cell interactions of outer membrane vesicle-associated virulence factors of enterohemorrhagic Escherichia coli O157: Intracellular delivery, trafficking and mechanisms of cell injury. *PLoS Pathog.* **13**, e1006159 (2017).

50. Bomberger, J. M. et al. Long-distance delivery of bacterial virulence factors by Pseudomonas aeruginosa outer membrane vesicles. *PLoS Pathog.* **5**, e1000382 (2009).
51. Veith, P. D. et al. Porphyromonas gingivalis outer membrane vesicles exclusively contain outer membrane and periplasmic proteins and carry a cargo enriched with virulence factors. *J. Proteome Res.* **13**, 2420–2432 (2014).
52. Minkeviciene, R. et al. Age-related decrease in stimulated glutamate release and vesicular glutamate transporters in APP/PS1 transgenic and wild-type mice. *J. Neurochem.* **105**, 584–594 (2008).
53. Koffie, R. M. et al. Apolipoprotein E4 effects in Alzheimer's disease are mediated by synaptotoxic oligomeric amyloid-beta. *Brain* **135**, 2155–2168 (2012).
54. Dinamarca, M. C., Rios, J. A. & Inestrosa, N. C. Postsynaptic receptors for amyloid-beta oligomers as mediators of neuronal damage in Alzheimer's disease. *Front Physiol.* **3**, 464 (2012).
55. Ittner, L. M. & Gotz, J. Amyloid-beta and tau–a toxic pas de deux in Alzheimer's disease. *Nat. Rev. Neurosci.* **12**, 65–72 (2011).
56. Jarosz-Griffiths, H. H., Noble, E., Rushworth, J. V. & Hooper, N. M. Amyloid-beta receptors: the good, the bad, and the prion protein. *J. Biol. Chem.* **291**, 3174–3183 (2016).
57. Hong, S. et al. Complement and microglia mediate early synapse loss in Alzheimer mouse models. *Science* **352**, 712–716 (2016).
58. Frisardi, V., Panza, F., Seripa, D., Farooqui, T. & Farooqui, A. A. Glycerophospholipids and glycerophospholipid-derived lipid mediators: a complex meshwork in Alzheimer's disease pathology. *Prog. Lipid Res.* **50**, 313–330 (2011).
59. Sun, G. Y. et al. Integrating cytosolic phospholipase A(2) with oxidative/nitrosative signaling pathways in neurons: a novel therapeutic strategy for AD. *Mol. Neurobiol.* **46**, 85–95 (2012).
60. Wender, M., Adamczewska-Goncerzewicz, Z., Szczech, J. & Godlewski, A. Myelin lipids in aging human brain. *Neurochem. Pathol.* **8**, 121–130 (1988).
61. Schilling, T., Lehmann, F., Ruckert, B. & Eder, C. Physiological mechanisms of lysophosphatidylcholine-induced de-ramification of murine microglia. *J. Physiol.* **557**, 105–120 (2004).
62. Takenouchi, T., Sato, M. & Kitani, H. Lysophosphatidylcholine potentiates Ca2+ influx, pore formation and p44/42 MAP kinase phosphorylation mediated by P2X7 receptor activation in mouse microglial cells. *J. Neurochem.* **102**, 1518–1532 (2007).
63. Sundaram, J. R. et al. Cdk5/p25-induced cytosolic PLA2-mediated lysophosphatidylcholine production regulates neuroinflammation and triggers neurodegeneration. *J. Neurosci.* **32**, 1020–1034 (2012).
64. Sheikh, A. M. & Nagai, A. Lysophosphatidylcholine modulates fibril formation of amyloid beta peptide. *FEBS J.* **278**, 634–642 (2011).
65. Sheikh, A. M., Michikawa, M., Kim, S. U. & Nagai, A. Lysophosphatidylcholine increases the neurotoxicity of Alzheimer's amyloid beta1-42 peptide: role of oligomer formation. *Neuroscience* **292**, 159–169 (2015).
66. Qin, Z. X., Zhu, H. Y. & Hu, Y. H. Effects of lysophosphatidylcholine on beta-amyloid-induced neuronal apoptosis. *Acta Pharm. Sin.* **30**, 388–395 (2009).
67. Esler, W. P. et al. Alzheimer's disease amyloid propagation by a template-dependent dock-lock mechanism. *Biochemistry* **39**, 6288–6295 (2000).
68. Karran, E., Mercken, M. & De Strooper, B. The amyloid cascade hypothesis for Alzheimer's disease: an appraisal for the development of therapeutics. *Nat. Rev. Drug Discov.* **10**, 698–712 (2011).
69. Yan, P. et al. Characterizing the appearance and growth of amyloid plaques in APP/PS1 mice. *J. Neurosci.* **29**, 10706–10714 (2009).
70. Hefendehl, J. K. et al. Long-term in vivo imaging of beta-amyloid plaque appearance and growth in a mouse model of cerebral beta-amyloidosis. *J. Neurosci.* **31**, 624–629 (2011).
71. Habchi, J. et al. Cholesterol catalyses Abeta42 aggregation through a heterogeneous nucleation pathway in the presence of lipid membranes. *Nat. Chem.* **10**, 673–683 (2018).
72. Yanagisawa, K. GM1 ganglioside and the seeding of amyloid in Alzheimer's disease: endogenous seed for Alzheimer amyloid. *Neuroscientist* **11**, 250–260 (2005).
73. Alarcon, J. M. et al. Ion channel formation by Alzheimer's disease amyloid beta-peptide (Abeta40) in unilamellar liposomes is determined by anionic phospholipids. *Peptides* **27**, 95–104 (2006).
74. Zhao, H., Tuominen, E. K. & Kinnunen, P. K. Formation of amyloid fibers triggered by phosphatidylserine-containing membranes. *Biochemistry* **43**, 10302–10307 (2004).
75. Lee, G., Pollard, H. B. & Arispe, N. Annexin 5 and apolipoprotein E2 protect against Alzheimer's amyloid-beta-peptide cytotoxicity by competitive inhibition at a common phosphatidylserine interaction site. *Peptides* **23**, 1249–1263 (2002).
76. Swasthi, H. M., Basalla, J. L., Dudley, C. E., Vecchiarelli, A. G. & Chapman, M. R. Cell surface-localized CsgF condensate is a gatekeeper in bacterial curli subunit secretion. *Nat. Commun.* **14**, 2392 (2023).
77. Ali, S. A. et al. Alzheimer's progenitor amyloid-beta targets and dissolves microbial amyloids and impairs biofilm function. *Adv. Sci. (Weinh.)* **10**, e2301423 (2023).
78. Bhoite, S. S., Han, Y., Ruotolo, B. T. & Chapman, M. R. Mechanistic insights into accelerated alpha-synuclein aggregation mediated by human microbiome-associated functional amyloids. *J. Biol. Chem.* **298**, 102088 (2022).
79. Williams, T. L. & Serpell, L. C. Membrane and surface interactions of Alzheimer's Abeta peptide–insights into the mechanism of cytotoxicity. *FEBS J.* **278**, 3905–3917 (2011).
80. Jung, A. L. et al. Legionella pneumophila outer membrane vesicles: isolation and analysis of their pro-inflammatory potential on macrophages. *J. Vis. Exp.* **120**, 55146 (2017).
81. Yang, Y. et al. High dose zinc supplementation induces hippocampal zinc deficiency and memory impairment with inhibition of BDNF signaling. *PLoS One* **8**, e55384 (2013).
82. Liu, J. et al. Plasma quantitative lipid profiles: identification of CarnitineC18:1-OH, CarnitineC18:2-OH and FFA (20:1) as novel biomarkers for pre-warning and prognosis in acute myocardial infarction. *Front. Cardiovasc. Med.* **9**, 848840 (2022).
83. Guo, S. et al. Comparative metabolic profiling of wild Cordyceps species and their substituents by liquid chromatography-tandem mass spectrometry. *Front. Pharm.* **13**, 1036589 (2022).

Acknowledgements

This work was supported by the National Natural Science Foundation of China (Grant number 82171426, 32300792); the Basic research program founded by Wuhan Science and Technology Bureau (grant no. 2023020201010196); the Science, Technology and Innovation Commission of Shenzhen Municipality (grant no. JCYJ20220530160805012).

Author contributions

J.Z. and R.L. initiated and designed the experiments and revised the manuscript. D.L.M. performed the experiments, analyzed the data, and wrote the manuscript. Y.W.L contributed a lot in brain microinjections and in vitro experiments. L.Z. and Z.D.X helped with animal experiments. W.T.H., H.W., and C.P.G. assisted with cell experiments. X.P.J. and H.Z. assessed with bacteria culture. R.X., L.P.Z., and S.Q.L. assisted with the intracellular

calcium imaging experiment, and Y.C. and X.C.W. gave constructive advice during experiments.

Competing interests
The authors declare no competing interests.

Additional information
Supplementary information The online version contains supplementary material available at https://doi.org/10.1038/s42003-024-07125-1.

Correspondence and requests for materials should be addressed to Rong Liu or Ji Zeng.

Peer review information *Communications Biology* thanks the anonymous reviewers for their contribution to the peer review of this work. Primary Handling Editors: Ibrahim Javed and Benjamin Bessieres. [A peer review file is available.]